PALEOCEANOGRAPHY, VOL. 7, NO. 6, PAGES 701-738, DECEMBER 1992

ON THE STRUCTURE AND ORIGIN OF MAJOR GLACIATION CYCLES
1. LINEAR RESPONSES TO MILANKOVITCH FORCING

J. Imbrie, [1] E. A. Boyle, [2] S. C. Clemens, [1]
A. Duffy, [1] W. R. Howard, [3] G. Kukla, [3]
J. Kutzbach, [4] D. G. Martinson, [3] A. McIntyre,[3,5]
A. C. Mix, [6] B. Molfino, [3] J. J. Morley, [3]
L. C. Peterson, [7] N. G. Pisias, [6] W. L. Prell, [1]
M. E. Raymo, [2] N. J. Shackleton, [8] and
J. R. Toggweiler [9]

Abstract. Time series of ocean properties provide a measure of global ice volume and monitor key features of the wind-driven and density-driven circulations over the past 400,000 years. Cycles with periods near 23,000, 41,000, and 100,000 years dominate this climatic narrative. When the narrative is examined in a geographic array of time series, the phase of each climatic oscillation is seen to progress through the system in essentially the same geographic sequence in all three cycles. We argue that the 23,000- and 41,000-year cycles of glaciation are continuous, linear responses to orbitally driven changes in the Arctic radiation budget; and we use the phase progression in each climatic cycle to identify the main pathways along which the initial, local responses to radiation are propagated by the atmosphere and ocean. Early in this progression, deep waters of the Southern Ocean appear to act as a carbon trap. To stimulate new observations and modeling efforts, we offer a process model that gives a synoptic view of climate at the four end-member states needed to describe the system's evolution, and we propose a dynamic system model that explains the phase progression along causal pathways by specifying inertial constants in a chain of four subsystems.

[1] Department of Geological Sciences, Brown University, Providence, Rhode Island.
[2] Department of Earth, Atmospheric, and Planetary Sciences, Massachusetts Institute of Technology, Cambridge.
[3] Lamont-Doherty Geological Observatory of Columbia University, Palisades, New York.
[4] Center for Climatic Research and Space Science, University of Wisconsin, Madison.
[5] Department of Geology, Queens College of CUNY, Flushing, New York.
[6] College of Oceanography, Oregon State University, Corvallis.
[7] Rosenstiel School of Marine and Atmospheric Science, University of Miami, Miami, Florida.
[8] Godwin Laboratory for Quaternary Research, Cambridge , United Kingdom.
[9] Geophysical Fluid Dynamics Laboratory, NOAA, Princeton, New Jersey.

Paper number 92PA02253
0883-8305/92/92PA-02253$10.00

> "Solutions to problems involving systems of such complexity are not born full grown like Athena from the head of Zeus. Rather they evolve slowly, in stages, each of which requires a pause to examine data at great lengths in order to guarantee a sure footing and to properly choose the next step."
>
> —Victor P. Starr

1. INTRODUCTION

What caused the Pleistocene ice ages? Since the middle of the nineteenth century, when geologists first tracked the expansion and retreat of ice sheets on land, this question has dominated research on past climates. Initially, the succession of glacial and interglacial ages appeared to be irregularly

spaced in time. However, during the 1960s and 1970s, when geologists learned to read and date the climatic record in ocean sediments, evidence mounted that glacial variability over the past half-million years exhibits a distinct pattern that is dominated by cycles with periods near 23,000, 41,000, and 100,000 years. This finding rekindled interest in the Milankovitch theory [Milankovitch, 1930] and led eventually to a demonstration that the astronomical cycles of precession, obliquity, and eccentricity [Berger, 1978a] are climatically important influences [Mesolella et al., 1969; Broecker and van Donk, 1970; Hays et al., 1976; Imbrie et al., 1984]. It is now widely believed that these astronomical influences, through their control of the seasonal and latitudinal distribution of incident solar radiation, either drive the major climate cycles externally or set the phase of oscillations that are driven internally.

The Pleistocene ice ages therefore provide an opportunity to test ideas about the mechanisms of the climate system's response to a known external forcing. Apart from the daily and annual cycles, such opportunities are rare. The numerical modeling community has responded to this opportunity by conducting a considerable number of experiments. Some of these use models of the general circulation (GCMs) to simulate the system's equilibrium response to a boundary condition fixed at some particular point in the cycle of radiation [Royer et al., 1984; Kutzbach and Guetter, 1986; Mitchell et al., 1988; Rind et al., 1989]. Others use low-order models to simulate the time-dependent response to a variable Milankovitch forcing [Le Treut and Ghil, 1983; Maasch and Saltzman, 1990; DeBlonde and Peltier, 1991; Gallée et al., 1992] or to examine the system's response to changes in a particular orbital parameter [Short et al., 1991].

Our purpose is to provide an array of observations showing how key parts of the system varied at Milankovitch frequencies over the past 400 kyr (kyr = 1000 years). Because the system also varies at higher and lower frequencies, we use standard techniques of spectral analysis to focus attention on the three main cycles. The same techniques have helped to identify and evaluate physical mechanisms that govern the semiannual, annual, quasi-biennial, and El Niño cycles [Rasmusson and Carpenter, 1982]. As applied to the Milankovitch problem, this approach allows us to compare the amplitude and phase of the forcing function in each Milankovitch cycle with the amplitude and phase of the system's response in a global array of sites. Finding that the response over much of our array forms a progressive wave that has the same basic geographic pattern in all three cycles, we then attempt to account for this simple cyclic structure by developing a conceptual model of the governing processes. Although we think that this model is physically plausible and hope that it will provoke useful discussion and stimulate new observational and modeling efforts, we make no claim that it is a unique way of explaining our observations or that we have explored all its implications in sufficient depth.

In particular, two predictions of our model cry out for additional testing against independent data. One prediction is that the initial response to external forcing is a change in the intensity of convection to intermediate depths in the Iceland gyre. In the modern ocean, dense waters produced in this way overflow the Denmark Strait and form the lower North Atlantic Deep Water (NADW). Although published information on the geological history of this key process strikes us as being consistent with the prediction, we know of no data which decisively confirm or deny it. The other prediction is that early in each glaciation cycle, deep waters of the Southern Ocean act as a carbon trap. Here there is a conflict in the evidence provided by two different indicators of carbon chemistry. Our model takes the evidence of $\Delta\delta^{13}C$ at face value and disregards the contrary indications given by observations of Cd/Ca at some sites.

One challenge in describing any model of the ice ages is to devise a comprehensible way of displaying information in a space of many dimensions. In our case, the number of dimensions exceeds 12: geographic position (3), time (1), frequency (3), insolation forcing (1+), and the climatic responses of ice sheets, surface ocean, subsurface ocean, and land (4+). Although we have done our best to simplify data display, readers will still be faced with a number of complex figures. However, two of our discoveries make it possible to present our model of the glaciation process in quite a compact way. First, the time evolution of the system can be described reasonably well in a space defined by four extreme end-member states. Second, the geographic sequence of responses in all three of the major cycles is essentially the same. This allows us to describe a single "generic" cycle.

2. SAMPLING STRATEGY

Our first task is to construct a geographic array of time series. Where should they be located? Early work on ice-age dynamics pointed to the importance of physical feedback mechanisms that operate at high latitudes: in the atmosphere, on land, and in various parts of the cryosphere and surface ocean [Birchfield and Weertman, 1983; Budd and Smith, 1987]. More recently, the dramatic demonstration in ice cores that glacial cycles are strongly correlated with atmospheric CO_2 made it clear that major changes in the carbon cycle — and therefore changes in deep ocean circulation — must also play a role in the ice age story [Neftel et al., 1982; Broecker, 1982; Barnola et al., 1987]. This discovery forced an expansion of observational and modeling strategies put forward to "solve" the ice age problem, with atten-

tion now focused on the export of NADW and on chemical changes in the Southern Ocean that are linked to this export [Broecker and Peng, 1989]. Our objective therefore is to build an observational array that monitors conditions at many different sites in a global, three-dimensional system. Practical considerations require that we emphasize ocean records.

How long should these time series be? Ideally, all time series in our array should cover an interval several times longer than the longest cycle of interest (the 100-kyr cycle). Unfortunately, it is not possible to attain this ideal. Suitable sediments are not preserved at many sites where geological observations are badly needed, and at several important sites where long records are in fact preserved, technical problems make it difficult to establish a time scale that is sufficiently accurate for our purpose. Faced with this challenge, the scientific community has responded with two quite different observational strategies, one based on ^{14}C, the other on $\delta^{18}O$. Each has its advantages and limitations. The first strategy uses ^{14}C dating of sedimentary sequences with high accumulation rates to build a high-resolution record of the past ~25 kyr. This yields precise information about the last glacial-to-interglacial transition over a wide range of sites — but provides no information about other time intervals, including transitions from interglacial to glacial states. The second strategy uses $\delta^{18}O$ to correlate and provide a chronology for long deep-sea records that extend back 500 kyr and beyond at open-ocean sites. This yields precise information about oceanic changes occurring at Milankovitch frequencies over long intervals of time but provides little information about changes occurring on time scales shorter than about 5 kyr.

Here we combine these strategies. In sections 4 and 5, we construct an $\delta^{18}O$-based array of climatic time series that monitors many parts of the system over the past 400 kyr at open-ocean sites. Then, in section 6.4, we fill in some critical gaps with a set of short, ^{14}C-based time series that allow us to examine details of the response during the last transition from a glacial to an interglacial state. We also include some $\delta^{18}O$-based time series that are too short for meaningful spectral analysis but allow us to examine the responses at key locations over the past 150 kyr. Because our focus is on the process of glaciation, we exclude low-latitude sites where previous work has shown that climate history is dominated by changes in the monsoon circulation [Prell and Kutzbach, 1987; McIntyre et al., 1989; Clemens et al., 1991]. In fact, this strategy may well exclude consideration of low-latitude processes that could be important in changing the concentrations of methane and water vapor in the atmosphere. To the extent possible, we select ocean records that monitor elements of the wind-driven and density-driven circulation along a N-S Atlantic section where synoptic chemical data from the modern ocean are available for comparison (section 4.5). We exclude from consideration any long ocean record that lacks a detailed $\delta^{18}O$ stratigraphy. To this ocean array, we add two time series of dust accumulation. These reflect continental aridity in China (Figure 1, variable 3) and Arabia (Figure 1, variable 4).

Most of the observations in this array have already been published. Our main contribution is to place these records on a common chronology and to analyze them statistically in exactly the same way. The entire data set of over 10,000 individual measurements is available in digital form as SPECMAP Archive 2 at the National Center for Atmospheric Research and at the National Geophysical Data Center, both in Boulder, Colorado. Nearly half of the archive is the set of $\delta^{18}O$ measurements that provide the stratigraphic framework.

3. MODELING STRATEGY AND PROSPECTUS

In this paper we concentrate on the 23-kyr and 41-kyr cycles of glaciation. These prove to be so strongly correlated with large changes in seasonal radiation that we regard them as continuous, essentially linear responses to the Milankovitch forcing. In a subsequent paper we will remove these linearly forced components from each time series and examine the residual response. The residual response is dominated by a 100-kyr cycle, which has twice the amplitude of the 23- and 41-kyr cycles combined. In the band of periods near 100 kyr, variations in radiation correlated with climate are so small, compared with variations correlated with the two shorter climatic cycles, that the strength of the 100-kyr climate cycle must result from the channeling of energy into this band by mechanisms operating within the climate system itself.

Our first objective here is to extract information from 16 long (~400 kyr) time series about the processes which govern the glacial cycles (sections 5.1 and 5.2). The main difficulty in achieving this objective is the small number of sites in our array (Figure 1). To emphasize this point, suppose that these sites were as densely distributed as they are in the GEOSECS and CLIMAP data bases we use to describe the modern, "interglacial" state (Figure 1b). We could then produce contoured sections showing the state of the system every few thousand years and (given suitable graphics in a large monograph) watch the system evolve through many cycles. In the absence of such a complete array, we must ask simpler questions. Following Einstein's dictum — as simple as possible but not simpler — we ask, What is the minimum number of end-member states needed to describe the system's response over the Milankovitch band? The answer will be determined by the phase structure of the system variables (Figure 2). As documented in section 5.3, most of the responses observed in our array of long time series fall

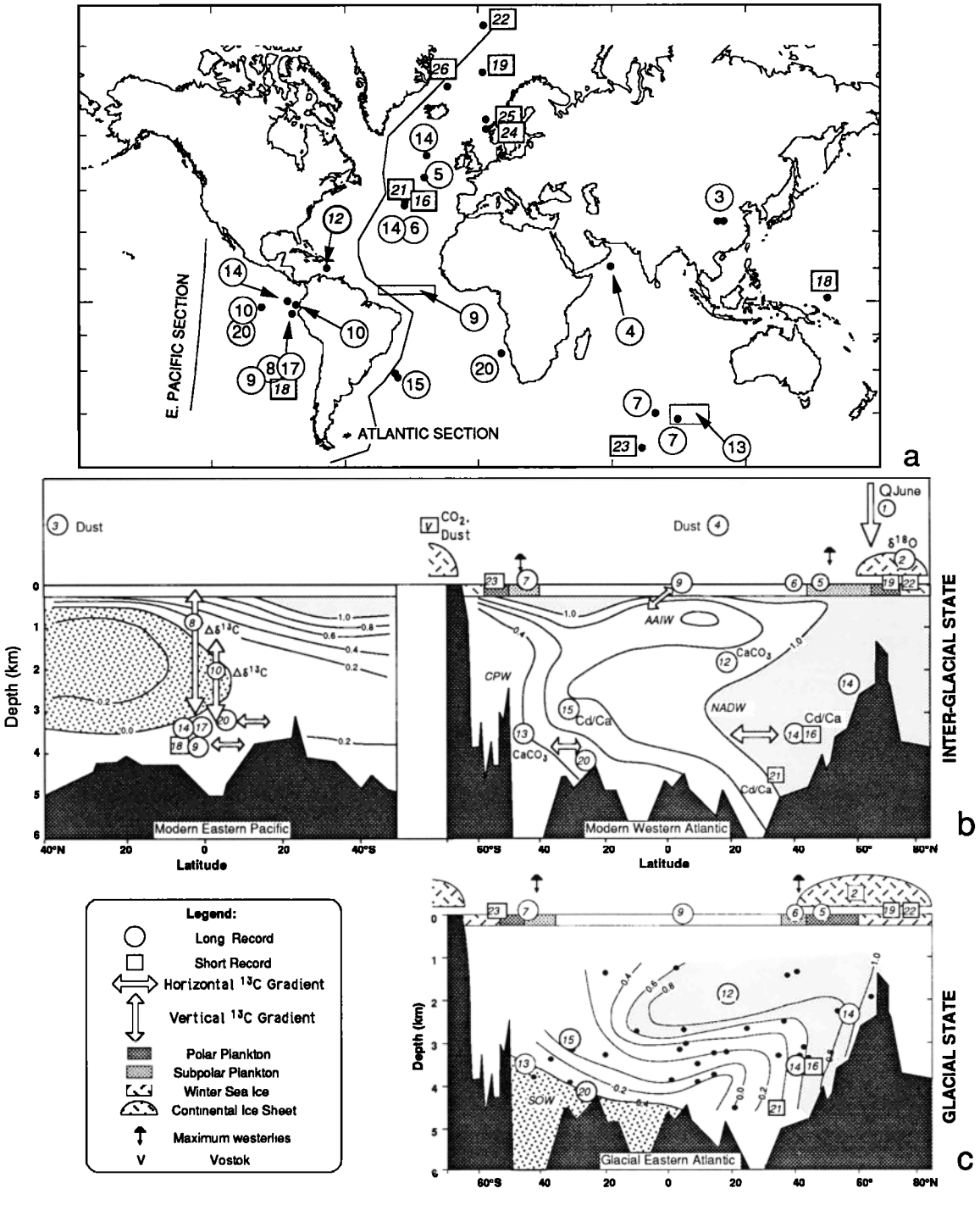

Fig. 1. A strategy for monitoring changes in climate linked to the Milankovitch cycles of glaciation and radiation. Measurements of ocean water and ocean sediments compiled along N-S sections (a) demonstrate that the geometry of atmospheric and oceanic flow today, when the system is in an interglacial state (b), is very different from the last glacial maximum, when the system was in a glacial state (c). To discover how the system oscillates between these states, 15 long time series spanning the past 400,000 years are arrayed near these sections. They include calculated variations in summer radiation at 65°N (variable 1), records of land ice (variable 2), atmospheric dust (variables 3, 4), and records of surface and deep ocean circulation documented in Table 1. Subsurface $\delta^{13}C$ data for (b) from Kroopnick [1985], for (c) from Duplessy et al. [1988], as recontoured by Broecker [1989]. Surface data from CLIMAP Project Members [1981], Howard and Prell [1992], and Keffer et al. [1988].

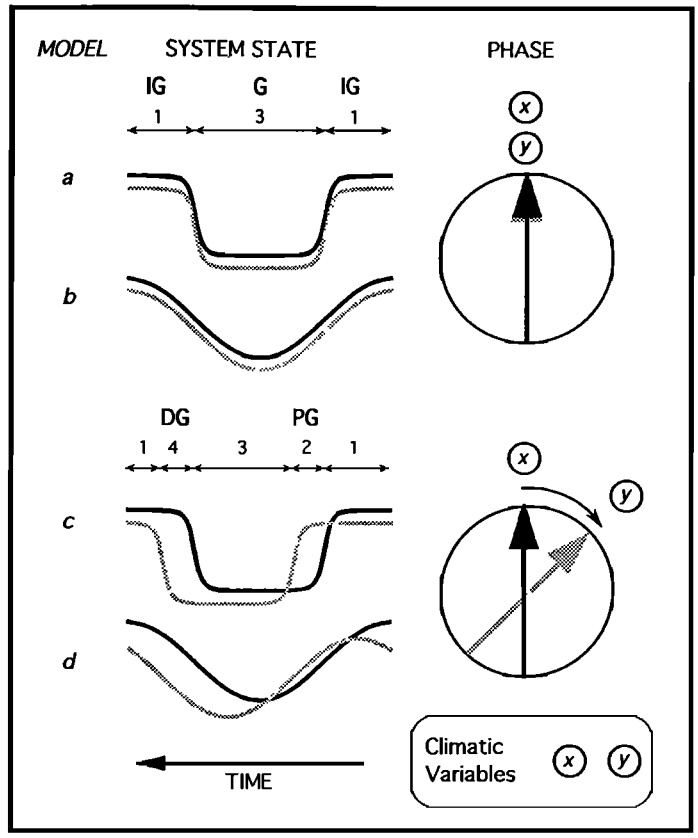

Fig. 2. Time-series models of a glacial-interglacial cycle with a single dominant period. In models a and b, the response of all variables to an unspecified forcing is in phase. This yields simultaneous, system-wide transitions between glacial (G) and interglacial (IG) states, and a symmetric state-sequence IG-G-IG-G (1-3-1-3...). In models c and d, the lagging phase of one set of variables (y) yields additional, preglacial (PG) and deglacial (DG) states, and an asymmetrical state-sequence IG-PG-G-DG (1-2-3-4...). These relationships hold for both square-wave (a, c) and sinusoidal (b, d) responses.

into two discrete phase clusters. We therefore conclude that much of the observed variability can be described in terms of four end-member states, which we refer to as the interglacial, preglacial, glacial, and deglacial states.

What processes govern the system's response at different phases of a cycle? Our answer is suggested by the major finding summarized in section 5.4. In most of the long records examined in this paper, the main features of the phase spectrum are the same in all three cycles: an early group of responses that leads ice volume, and a late group that is on phase with or slightly lags ice volume. Although the initial responses are not represented in our long time series, it is clear from the phase of responses in the precession and obliquity bands that these responses must occur at high northern latitudes (section 6.3), an inference for which we find support in some ^{14}C-dated records (section 6.4).

The entire phase sequence is the basis for a process model (described in section 6.5 and summarized in Figure 3) that identifies the main pathways along which climatic changes are propagated. This model emphasizes the ocean's role as a heat pump and focuses on two different pathways along which warm-to-cold-water conversion occurs. Some of the conversion occurs in the open waters of the North Atlantic Ocean, and some in more restricted waters of the Nordic Sea (a term we will use to describe the Iceland, Norwegian, and Greenland seas [Hurdle, 1986; McCartney, 1992]). These pathways are (1) open-ocean convection in the boreal Atlantic ("boreal heat pump") and (2) overflow of intermediate waters from the Nordic Sea into the Atlantic basin ("Nordic heat pump"). Lehman and Keigwin [1992a, b] refer to these pathways as the upper and lower belts of the global conveyor circulation [Broecker, 1990].

We consider our model, which describes the system's evolution in terms of four end-member states, to be an extension of a simpler conceptual model developed by Broecker et al. [1985] and Broecker and Denton [1989]. We envision a system varying

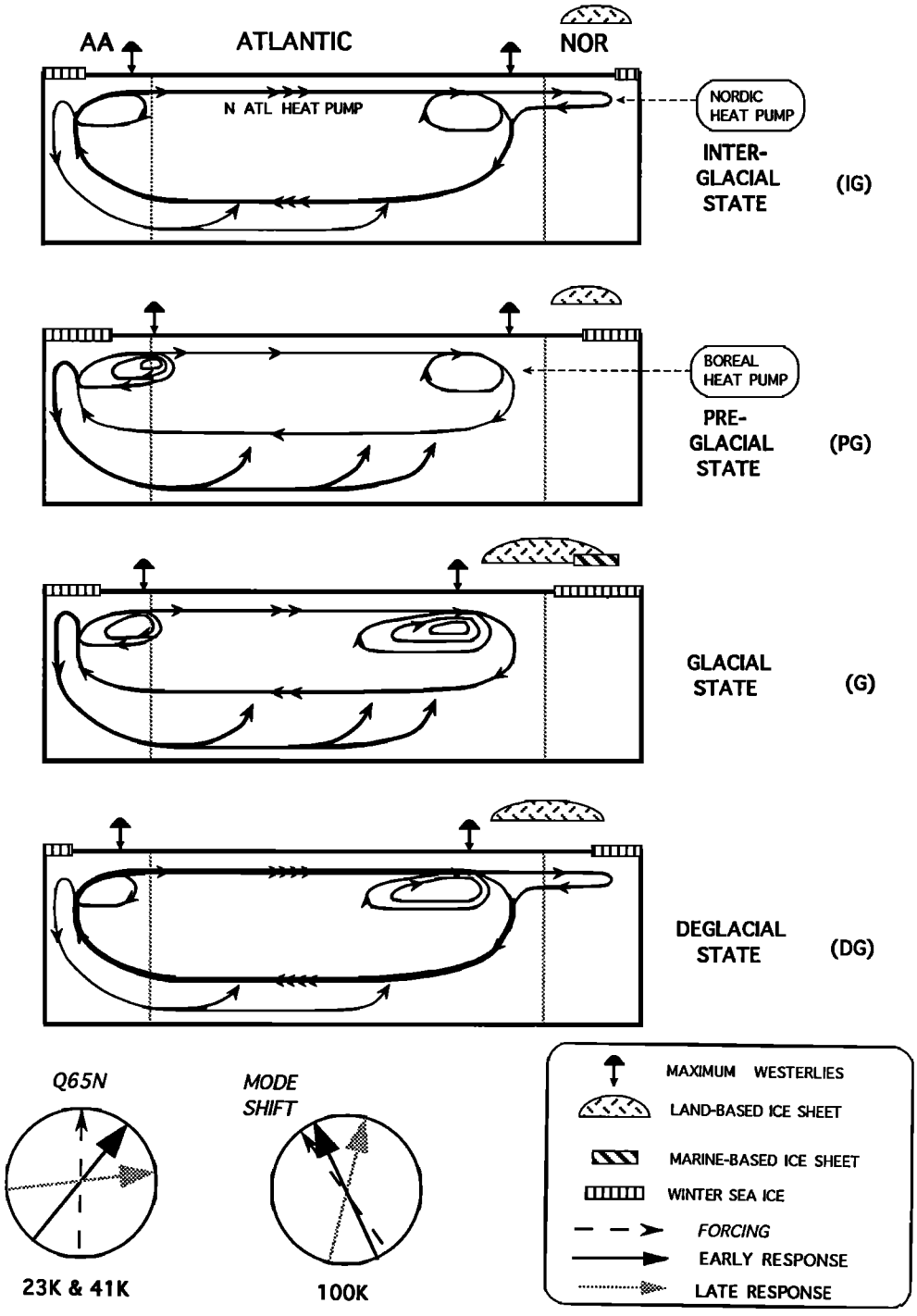

Fig. 3. Process model of a generic Milankovitch glaciation cycle showing the main pathways along which climatic variance is propagated. Unlike the simple model in Figure 2, the actual glacial-interglacial cycle is compound: the sum of 23-kyr, 41-kyr, and 100-kyr cycles that have similar phase progressions. Top four panels: N-S sections through the Nordic Sea (NOR), Atlantic Ocean, and Antarctic Ocean (AA) showing key elements of the surface and subsurface circulation and the geometry of sea ice and ice sheets at different states of the glaciation cycle. The strength of the global overturning circulation (N. Atlantic heat pump) is shown by line thickness. Warm-to-cold-water conversion occurs in two branches of this flow: (1) the boreal heat pump (open-ocean convection in the boreal Atlantic); and (2) the Nordic heat pump (overflow of Nordic intermediate waters). The strength of wind- and density-driven overturnings within the Antarctic and Atlantic is shown by schematic stream function contours. Bottom panel: summary of the observed phase pattern (Figure 10) used to construct this model. In the 23-kyr and 41-kyr bands, June radiation at 65°N is the forcing (dashed vector); in the 100-kyr band, the forcing is a shift in the mode of ocean overturning.

among four states and (as shown in Figure 4) exhibiting shifts between two modes of circulation. Each mode is identified with a particular part of the warm-to-cold-water conversion process in the North Atlantic that makes its own contribution to the total NADW export flux [McCartney and Talley, 1984; Lehman and Keigwin, 1992a, b]. One mode shift (from a one-pump to a two-pump mode) occurred about 14,000 (radiocarbon) years ago as the system changed rapidly from a glacial, through a deglacial,

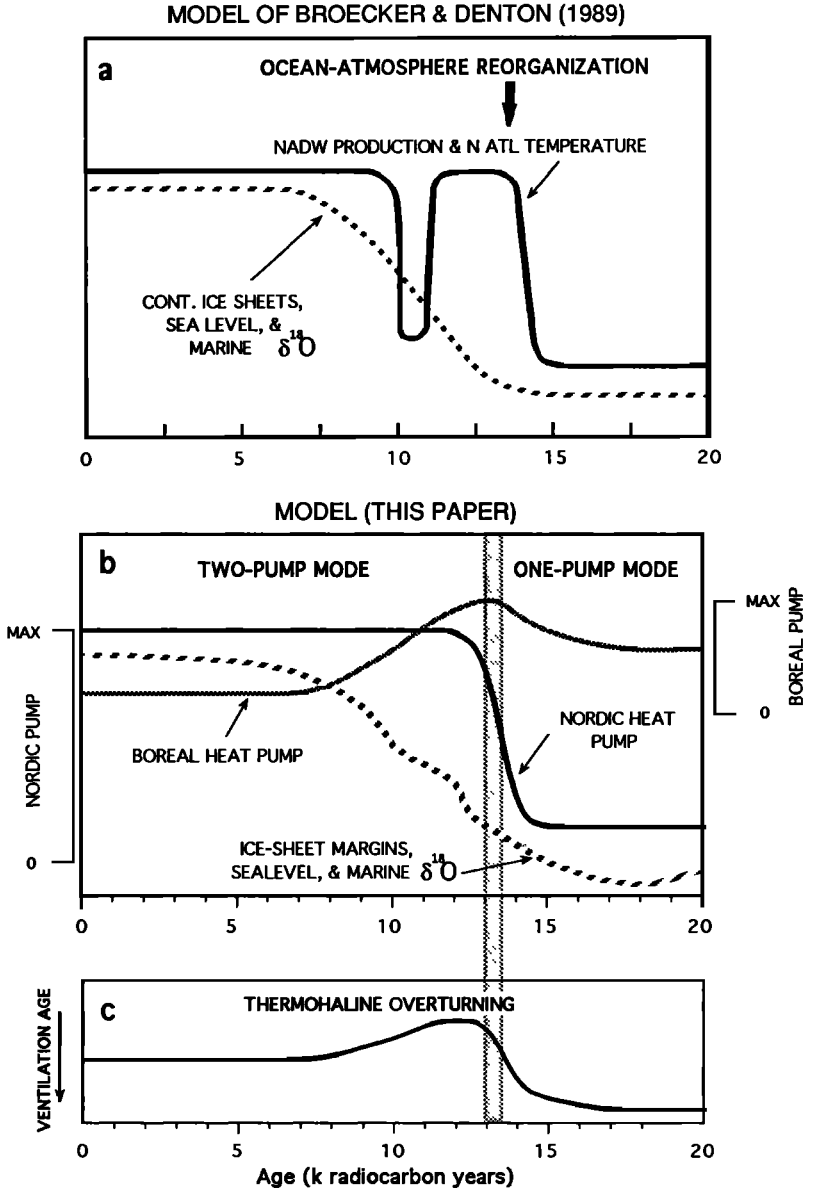

Fig. 4. Models of circulation modes. (a) Model identifying a major reorganization of the ocean-atmosphere system as the cause of the transition from a glacial to an interglacial state. The glacial state reflects a stable circulation mode in which the production of NADW and its transport out of the Atlantic are relatively slow. The mode switch may be driven by orbitally induced changes in salinity that are uncorrelated with the ice sheets and sea level. (b) A model (this paper) identifying this reorganization as a change from a one-pump to a two-pump mode of ocean overturning. The mode switch is driven by orbitally induced changes in salinity that are linked to small changes in the wind field, ice sheet margins, and sea level. (c) Rate of global overturning resulting from the combined action of the Nordic and boreal heat pumps. Early in the deglaciation process, when winds still strongly influenced by ice sheets continue to drive the boreal pump after the Nordic pump has been turned on, overturning is more rapid than at present (in line with observations on the ventilation age of Pacific deep water).

to an interglacial state (Figures 3 and 4). A mode shift in the opposite direction (from a two-pump to a one-pump mode) occurred near the end of the last interglacial (Stage 5e) as the system shifted from an interglacial through a preglacial toward a glacial state. By suggesting how the two mechanisms would reinforce each other early in the deglaciation process, our model accounts for ^{14}C evidence that thermohaline overturning during deglaciation was much faster than it is today [Shackleton et al., 1988; Duplessy et al., 1991a]. The model predicts that the overturning and heat flux would be even slower in a preglacial state than it is in a glacial state (Figure 3).

As a final step in developing our ideas about the governing processes, we consider what sources of inertia are required to explain the observed phase sequence. In section 6.6, these inferences are formalized as time constants in a quantitative, four-component system model.

4. METHODS

4.1. *Stratigraphy and Chronology*

Records of $\delta^{18}O$ make two important contributions to our study (Figure 5). First, they provide a single, global index of the intensity of continental glaciation by combining the dominant, ice volume effect with a smaller temperature effect [Shackleton and Opdyke, 1973]. By stacking many records, we obtain an index in which local temperature effects are reduced [Imbrie et al., 1984]. Second, because the $\delta^{18}O$ meltwater signal from the ice sheets is mixed rapidly around the ocean [Duplessy et al., 1991a], these records also provide a basis for determining how local changes in other climate variables relate in time to changes in the global index. The precision of this determination — and therefore the uncertainty in dating events at one site with respect to events at other sites — is limited by the mixing time of the ocean (~1 kyr) and the sampling rate of our cores, which averages about 3 kyr (Table 1). We are therefore able to provide a chronology for individual events which has an average uncertainty on the order of ±2.5 kyr with respect to any chronology that might be adopted for the $\delta^{18}O$ stack. In this paper we use the chronology of Imbrie et al. [1984].

4.2. *Spectra and Cross Spectra*

Why go to the trouble of transforming time series into the frequency domain? Why bother to calculate spectra? Our answer is that a statistical approach of this kind is made necessary by the incompleteness of our knowledge of the climate system's response to changes in the annual radiation cycle. If this knowledge were much better than it is, we could proceed in the time domain by testing quantitative predictions that integrate the system's response to this forcing over all latitudes, all seasons, and all Milankovitch frequencies. However, in the absence of such knowledge, spectral methods provide a way of partitioning a large and difficult problem into smaller units that are easier to understand.

The statistical methods we use to achieve this partitioning in the frequency domain (spectra) and in the time domain (filters) have been adapted from standard procedures used in meteorology and oceanography [Imbrie et al., 1989]. After interpolating each record at a constant time interval, we first estimate the variance-density spectrum of each variable and then calculate coherency and phase spectra of each variable against $\delta^{18}O$. The variance spectrum shows how much of the variance in a given signal is concentrated in different frequency bands. The coherency spectrum shows the extent to which the local and $\delta^{18}O$ signals are linearly correlated in each frequency band (when any phase difference between them is set to zero). If the coherency in a particular band is large enough to be statistically significant, we then ask what the phase of each local signal is with respect to $\delta^{18}O$. This information is summarized in a phase spectrum.

The particular numerical procedures we use are based on the relatively low-resolution (Blackman-Tukey) method. Although higher resolution methods are now available, we consider the lower-resolution method to be a useful buffer against chatter produced by dating uncertainties [Jenkins and Watts, 1968]. Experiments with a high-resolution (multiple-taper) method confirm the results as reported here. For consistency, phase angles and coherencies of each variable are calculated against the stacked $\delta^{18}O$ record (Table 2). These estimates are not statistically different from those calculated against the local $\delta^{18}O$ signal and have narrower confidence intervals. The phase and coherency of the stacked $\delta^{18}O$ signal are calculated against a time series of orbital variations that control radiation in each band. Variance-density spectra are then transformed into amplitude-density spectra so that the relative heights of peaks correspond to the amplitudes of oscillations observed in time series. With this transformation, areas under the spectrum are not proportional to amplitude. The total amplitude of the variation at each frequency is shown, as well as the fraction that is coherent with (i.e., proportional to) variations in $\delta^{18}O$.

4.3. *Filters*

Having examined a climatic signal in the frequency domain and determined how much of its variance is concentrated in a particular Milankovitch cycle, we may wish to see that cycle in the time domain so that the amplitudes and phases of the individual oscillations can be placed in a stratigraphic context. This is done by applying an appropriate band-pass filter. The procedure we use involves convolution with a Tukey filter [Jenkins and

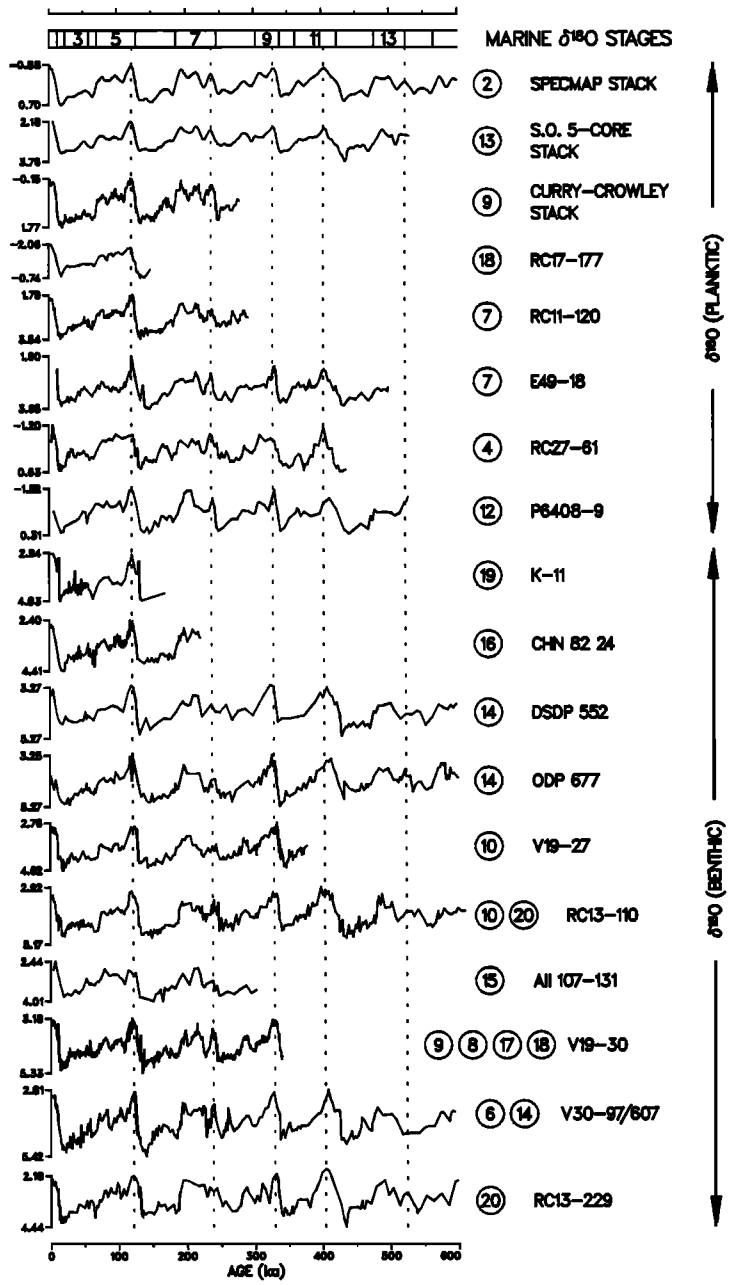

Fig. 5. Stratigraphy and chronology. The $\delta^{18}O$ record (in per mil) from each deep-sea core investigated in this paper is correlated against variable 2, a stratigraphic standard defined in Prell et al. [1986] as the SPECMAP stack. This correlation, accomplished by aligning characteristic events, transfers to each core whatever chronology is adopted for the standard — in this case, the chronology of Imbrie et al. [1984].

Watts, 1968]. When this operation is carried out in the normal way, the ends of each filtered record, including the Holocene portion, are lost [Hays et al., 1976]. To avoid this, we have used cyclic convolution procedures [Meskó, 1984] that provide estimates for the entire time span of each signal, including the ends. Because these end segments have substantial uncertainties, we identify them with special symbols in section 5.3.

4.4. *Phase Errors and Climatic Noise*

Each phase estimate given in Table 2 is the mean phase difference measured between a local climatic

TABLE 1. Description of Climatic Records

Number	Record	Data	Reference	Latitude, deg	Longitude, deg	Depth, m	T, kyr	TS, kyr
1	Radiation	June Q↓	Berger [1978a, b]	65 N	--	--	610	--
2	Five-core stack	$\delta^{18}O$(plank.)	Imbrie et al. [1984]	--	--	3100	610	3.0
3	Three-site stack[a]	Magn. suscept.	Kukla et al. [1990]	36 N	109 E	- 1240	610	1.8
4	RC27-61	Dust flux	Clemens and Prell [1990]	17 N	60 E	1893	432	3.2
5	K708-1	SST (Foram)	Ruddiman and McIntyre [1984]	50 N	24 W	4053	260	1.4
6	V30-97/DSDP607	SST (Foram)	Ruddiman et al. [1989]	41 N	33 W	--	600	2.1
[6]	V30-97	SST (Foram)	Ruddiman and McIntyre [1981]	41 N	33 W	3371	240	1.3
[6]	DSDP607	SST (Foram)		41 N	33 W	3427	360	3.4
7	RC11-120/E49-18	SST (Rad)	Hays et al. [1976]; Morley [1989b]	44 S	80 E	--	498	1.6
[7]	RC11-120	SST (Rad)	Howard and Prell [1992]	44 S	80 E	3193	290	1.6
[7]	E49-18	SST (Rad)		46 S	90 E	3254	208	1.7
8	V19-30[b]	$\Delta\delta^{13}C$ (srf-deep)	Shackleton and Pisias [1985]	3 S	83 W	3091	343	0.6
9	Five-core stack[c]	$\Delta\delta^{13}C$ (srf-deep)	Curry and Crowley [1987]	6 N	41 W	3019	280	3.4
10	V19-27[d]	$\Delta\delta^{13}C$ (int-deep)	Mix et al. [1991]	0	82 W	1373	366	1.6
[10]	RC13-110	$\delta^{13}C$ (benthic)	Mix et al. [1991]	0	96 W	3231	535	2.6
12	P6408-9[e]	CO_3 diss. index	Peterson and Cofer-Shabica [1987]	15 N	69 W	4098	610	5.0
13	Five-core stack[f]	CO_3 pres. index	Howard and Prell [1990]	~45 S	~95 E	3400	492	4.2
14	DSDP607[g]	%NADW	Raymo et al. [1990]	41 N	33 W	3427	530	3.7
[14]	DSDP607	$\delta^{13}C$ (benthic)		41 N	33 W	3427	530	3.4
[14]	DSDP552	$\delta^{13}C$ (benthic)		56 N	23 W	2301	530	5.5
[14]	ODP677	$\delta^{13}C$ (benthic)		1 N	84 W	3461	530	3.1
15	AII107-131/-65[h]	Cd/Ca	Boyle [1984a, b]	31 S	37 W	2860	302	4.4
[15]	AII107-131	Cd/Ca	Jones et al. [1984]	31 S	38 W	2925	302	4.9
[15]	AII107-65	Cd/Ca		32 S	36 W	2795	118	2.4
16	CH82-24-4PC	Cd/Ca	Boyle and Keigwin [1985]; and this paper	42 N	33 W	3427	219	1.1

TABLE 1. (continued)

Number	Record	Data	Reference	Latitude, deg	Longitude, deg	Depth, m	T, kyr	TS, kyr
17	V19-30	$\delta^{13}C$ (benthic)	Shackleton and Pisias [1985]	3 S	83 W	3091	343	0.6
18	RC17-177[i]	$\delta^{18}O$ (plank.)	Shackleton [1987]	2 N	159 E	2600	138	3.5
19	K-11	$\delta^{18}O$ (plank.)	Kellogg et al. [1978]	72 N	2 E	2900	134	1.6
20	$\delta^{13}C$ gradient[j]	$\Delta\delta^{13}C$ (deep-deep)		--	--	--	535	3.0
[20]	RC13-229	$\delta^{13}C$ (benthic)	Oppo et al. [1990]	26 S	11 E	4194	607	5.5
21	EN120-GGC-1	Cd/Ca	Keigwin et al. [1991]	34 N	58 W	4450	15	0.1
22	PS21295-4	$\delta^{18}O$ (plank.)	Jones and Keigwin [1988]	78 N	2 E	3112	16	8.2
23	MD84-551	SST (diatoms)	Bard et al. [1990b]	55 S	73 E	2230	30	1.2
24	Troll 3.1	Forams	Lehman and Keigwin [1992a]	61 N	4 E	332	15	0.2
25	HM79-6/4	Diatoms	Karpuz and Jansen [1992]	63 N	3 E	900	14	0.2
26	57-5	Diatoms	Karpuz and Schrader [1990]	69 N	13 W	1892	10	1.1

Core location, depth below sea level, time span (T), and mean time-sampling interval (TS). The [ ] indicates individual records combined to form a single climatic index by patching, stacking, or differencing. Sea surface temperature (SST) estimates are for the warm season based on counts of planktonic foraminifera, radiolaria, or diatoms.

[a]Observations reflect aridity on the Chinese loess plateau.

[b]Benthic values of $\delta^{13}C$ (*Uvigerina senticosta*) are subtracted from planktonic values (*Neogloboquadrina dutertrei*).

[c]Benthic values of $\delta^{13}C$ in variable 17 are subtracted from a stacked record of planktonic $\delta^{13}C$ (*Globigerinoides sacculifer*) obtained from cores between 40°N and 11°N, and 20°W to 79°W. The tabled location and depth are average values for the five records.

[d]Values of $\delta^{13}C$ in V19-27 minus values in RC13-110. Both datasets on *Cibicides wuellerstorfi*.

[e]An index based on percent of foram fragments. $\delta^{18}O$ stratigraphy from Emiliani [1978].

[f]Preservation index for five cores between 42°S and 48°S at depths between 3206 m and 3863 m.

[g]Index of ventilation at site 607 formed by comparing $\delta^{13}C$ fractionation there with values at end-member sites 552 (N. Atl.) and 677 (Pac.).

[h]For the interval 57 to 70 ka, data from AII107-65 are patched in to AII107-131 based on $CaCO_3$ and $\delta^{18}O$ correlations.

[i]Planktonic $\delta^{18}O$ values in this core are subtracted from benthic values in core 17 to estimate bottom temperature at that site.

[j]Values of $\delta^{13}C$ in RC13-229 (variable 20) minus values in RC13-110 (variable 10). Both data sets on *Cibicides wuellerstorfi*.

TABLE 2. Statistical Summary of Cross Spectra of Climatic Time Series

Number	Variable	100 kyr		41 kyr		23 kyr		k_o	T	Δt
		k	ø, deg	k	ø, deg	k	ø, deg			
1	Q↓ 65°N June	—	—	0.91	- 78 ± 11	0.95	- 86 ± 9	0.66	400	2
2	Stack -$\delta^{18}O$	0.91	+13 ± 12	0.90	+80 ± 12	0.95	+87 ± 9	0.66	400	2
3	-China loess	0.89	+19 ± 13	0.79	+16 ± 20	0.69	+12 ± 26	0.66	400	1
4	-Arab. dust	0.96	+10 ± 8	0.80	+1 ± 19	0.94	+4 ± 9	0.66	400	2
5	K708-1 SST	0.99	+6 ± 2	0.98	+12 ± 6	0.91	+27 ± 15	0.82	260	2
6	V3097/607 SST	0.85	+3 ± 16	0.95	- 13 ± 9	0.94	+72 ± 9	0.66	400	2
7	SST 44°S	0.92	- 47 ± 11	0.93	- 14 ± 10	0.86	- 35 ± 15	0.66	400	2
8	$-\Delta\delta^{13}C$ (s-deep)	0.91	- 44 ± 13	0.89	- 32 ± 15	0.91	- 39 ± 12	0.71	343	1
9	$-\Delta\delta^{13}C$ (s-deep)	0.87	- 41 ± 18	0.88	- 57 ± 17	0.81	- 8 ± 22	0.79	280	1
10	$-\Delta\delta^{13}C$ (i-deep)	0.72	- 26 ± 25	0.76	+13 ± 23	(0.42)	+130 ± 46	0.69	366	3
12	CO_3 diss. Carib.	0.82	- 1 ± 18	0.92	+13 ± 11	0.76	- 1 ± 21	0.66	400	5
13	CO_3 pres. 45°S	0.91	- 12 ± 12	0.89	- 38 ± 13	0.91	+7 ± 12	0.66	400	2
14	$\Delta\delta^{13}C$ (%NADW)	0.87	+16 ± 15	0.86	+5 ± 16	0.83	+41 ± 17	0.66	400	3
15	-Cd/Ca 31°S	0.92	- 77 ± 13	0.78	- 49 ± 23	0.80	- 27 ± 22	0.76	302	5
17	$\delta^{13}C$ (deep)	0.92	- 14 ± 12	0.92	- 9 ± 12	0.95	+10 ± 10	0.71	343	1
20	$\Delta\delta^{13}C$ (deep-deep)	0.82	- 34 ± 18	0.84	- 36 ± 16	0.93	- 56 ± 10	0.66	400	3

The signs of certain time series are changed to yield a definition of phase consistent with plotting conventions on Figure 7. Values for variable 2 are calculated versus eccentricity, obliquity, and the precession index (-e sin ω). Other variables are crossed with variable 2 (SPECMAP Stack $\delta^{18}O$). Positive phases indicate that the named variable lags the reference variable. Bandwidth for all calculations is 0.01 kyr^{-1}. Items tabled are: coherency (k); phase angle (ø) with 80% confidence interval; 80% test statistic for nonzero coherency (k_o); age in ka of oldest sample used in the calculation (T); and uniform sampling interval (Δt) in kiloyears. The ( ) indicates a value of k that is not significant at the 80% level. Statistical analysis has not been performed on time series shorter than 260 kyr.

proxy and $\delta^{18}O$ over the past 400 kyr (or over the core length T, if T is less than 400 kyr). The observed range of phase differences around each mean is reported as an 80% confidence interval by making standard assumptions of normality [Jenkins and Watts, 1968]. These confidence intervals must reflect two different sources of phase variability: phase differences due to correlation errors (analytical noise) and phase differences due to an irregularity in the climatic process (climatic noise).

What fraction of the confidence intervals reported in Table 2 can be attributed to analytical noise and what fraction to climatic noise (i.e., natural climatic variability)? The main component of analytical noise is the error in correlating climatic records. Owing to low sampling rates, bioturbation, or local changes in $\delta^{18}O$, the actual correlation error for isotopic events in some cores may exceed the average error estimated in section 4.1 (±2.5 kyr) by several kiloyears. Martinson et al. [1987], who investigated this error using a variety of climate records and correlation criteria, estimate that the total range of errors averages ±5 kyr. It is therefore important to base estimates of phase differences between cores on procedures which integrate over substantial intervals. Our cross-spectral estimates versus $\delta^{18}O$ are averaged over the entire length of each core; estimates based on digital filters are averaged over a sliding interval of ~100 kyr. For most cores, this averaging of random noise would yield mean errors on the order of ±1°, ±2°, and ±4°, respectively, for the 100-, 41-, and 23-kyr cycles. These estimates of analytical noise are much smaller than the total observed ranges that are reported in Table 2 as 80% confidence intervals (~±15° for each cycle). The confidence intervals are therefore mainly a record of climatic noise. Expressed in terms of a $\pm 2\sigma$ range in time, the level of climatic noise in the 100-kyr cycle is quite large (~16 kyr) compared to the 23-kyr cycle (~4 kyr).

4.5. *Proxy Ocean Variables*

The main objective of our sampling program is to obtain time series of ocean-sediment properties that record key features of the wind-driven and density-driven circulations. The proxy indicators we use to infer these patterns are documented in Table 1 and illustrated in Figures 1 and 6. The following paragraphs are written for readers who are unfamiliar with these methods. Readers impatient to see our results should go on to section 5.

Like inversion methods used to infer flow patterns in the modern ocean from the observation of water properties, proxy methods in paleoclimatology have uncertainty ranges that may (or may not) be reduced significantly in a given circumstance by the specification of independent constraints. We use four different procedures, each calibrated against observations of modern sediment properties:

1. At high-latitude sites in the open ocean, the relative abundance of polar, subpolar, and subtropical plankton assemblages is used to infer the position of fronts and the temperature of surface waters (variables 5, 6, 7). In the Norwegian Sea, the abundance of a species of plankton that is characteristic of the open subpolar Atlantic is used as an index of the intensity of the exchange of water between the open Atlantic and this marginal sea (variable 19) [Kellogg, 1976; Kellogg et al., 1978]. Inferences about frontal position are based on the spatial distribution of modern assemblages (Figure 1b). The boundaries between these assemblages are sharp because they are ecologically linked to frontal features of the surface circulation near the margins of cyclonic and anticyclonic gyres [Kellogg, 1976; McIntyre et al., 1976; Prell et al., 1979; Pichon et al., 1987; Howard and Prell, 1992]. These boundaries are therefore linked to the wind field. Because the spatial sequence of these assemblages in the modern and ice age ocean are the same, geographic shifts of these boundaries are reliable indicators of changes in the wind-driven circulation. However, for time series analysis we need a calibration that will allow us to express multivariate changes in the biota as a single objective index [Kipp, 1976; Prell, 1985]. Calibration against sea surface temperature (SST) provides the simplest as well as the most ecologically consistent and physically meaningful way of scaling these faunal time series. Alternate calibration schemes give essentially the same result [Molfino et al., 1982; Morley, 1989a; Pichon et al., 1992].

2. Gradients of $\delta^{18}O$ ($\Delta\delta^{18}O$) are used in certain circumstances (variable 18, Table 1) to infer the temperature of deep water [Shackleton, 1987], and in other circumstances (variable 22, Table 1) to infer the salinity of marginal seas [Jones and Keigwin, 1988].

3. Measurements of $\delta^{13}C$ in benthic foraminifera from Pacific deep water (variable 17) are used to estimate the average oceanic $\delta^{13}C$. To first order, fluctuations in this record reflect the transfer of organic carbon between dissolved-oceanic and continental-biomass reservoirs [Shackleton, 1977]. Because positive excursions of this curve can be explained by increases in continental biomass, this oceanic record can be interpreted as an index of conditions on land.

4. Gradients of $\delta^{13}C$ ($\Delta\delta^{13}C$) between two sites (variables 10, 14, 20), or between benthic and planktonic species at one site (variables 8, 9) are used to infer nutrient gradients between different water masses (double-headed arrows in Figure 1b). While this method does not yield absolute nutrient concentrations, owing to uncertainties in the time history of the global budget of $\delta^{13}C$ in the ocean, it does give a sense of the relative ages of deep water masses because deep-sea $\delta^{13}C$ and apparent oxygen utilization are correlated [Kroopnick, 1985]. Following a suggestion by Broecker [1982], Curry and Lohmann [1982] and Shackleton et al. [1983] were the first to use

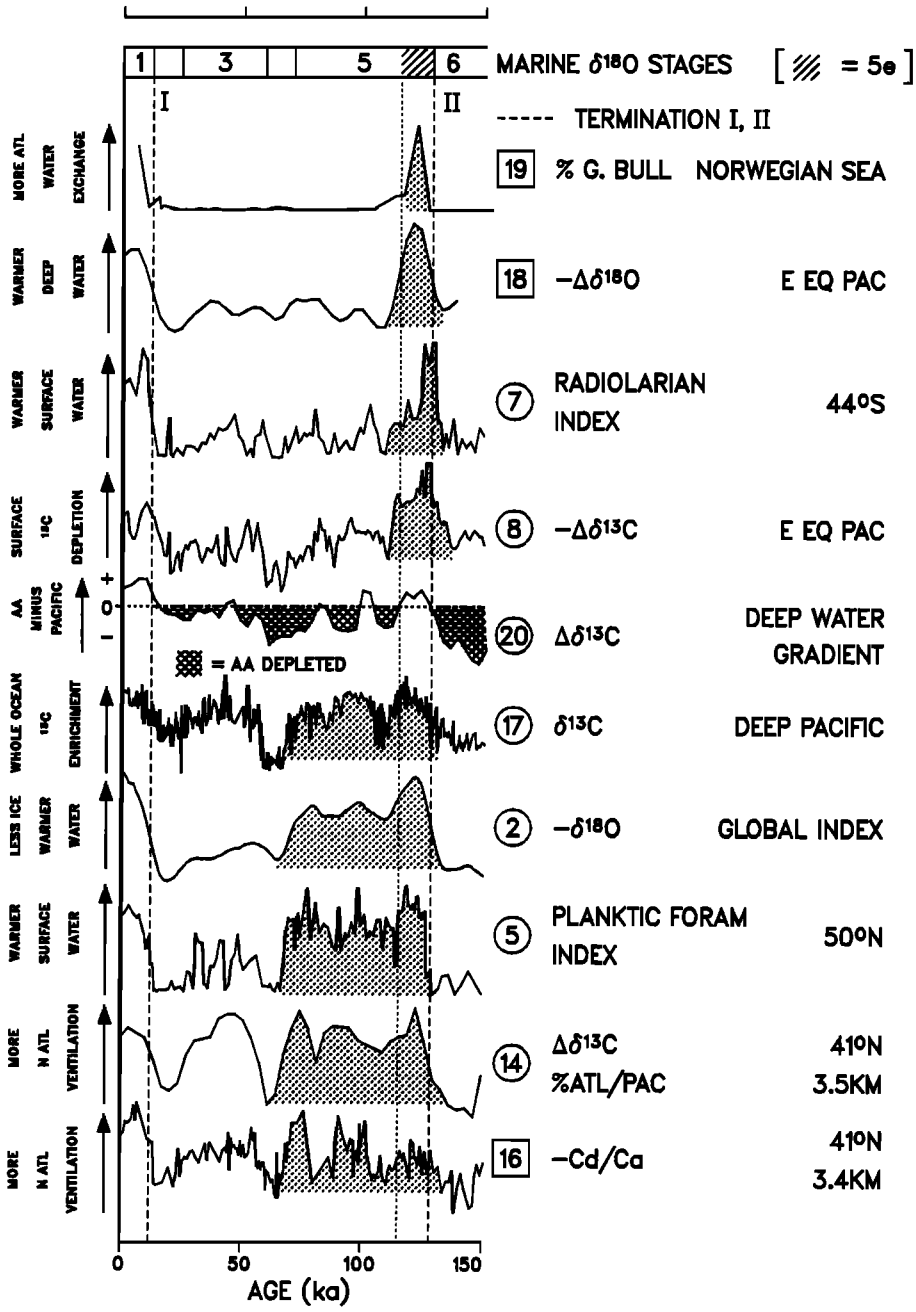

Fig. 6. Patterns of climate change over the past 150,000 years. The signs of observations identified on the right are reversed as needed so that the interpretation of each time series has a positive upward sense of change toward an interglacial condition (Table 1). For variable 20, for example, an upward shift in the curve means that deep waters in the Antarctic are becoming more enriched than in the Pacific. Widespread, positive transitions at Terminations I and II, lead to conditions that are generally near full interglacial values during Stages 1 and 5e. This synchronous pattern fits the two-state model of Figure 2a. However, negative transitions exhibit two distinct patterns, emphasized by shading. Variables 19, 18, 7, and 8 move decisively toward negative values near the end of Stage 5e, yielding "short interglacials"; whereas the global $\delta^{18}O$ index and variables 17, 5, 14, and 16 have "long interglacials" which end at Stage 4. This pattern of progressive transitions fits the four-state model of Figure 2c. In spectral analysis, the "short" and "long" patterns will appear as early and late phases of the 100-kyr cycle, with the phase of variable 20 in an intermediate position. Thus the time series as displayed here are actually in the order of this phase sequence (Table 2).

$\delta^{13}C$ gradients as indicators of deep-water chemistry and flow. Here an assumption is made that no major spatial changes in $\delta^{13}C$ of organic matter raining into the deep sea occurred in the past. Boyle [1990] raises the possibility that changes in $\delta^{13}C$ of Antarctic plankton could induce local bias in $\delta^{13}C$-based estimates of deep-sea ventilation.

5. The $\delta^{13}C$ evidence of ocean chemistry can be supplemented by measurements of Cd/Ca (variables 15, 16) and $CaCO_3$ dissolution (variables 12, 13) [Boyle and Keigwin, 1982; Boyle, 1984a; Crowley, 1985]. In principle, the addition of $\delta^{13}C$-depleted carbon to the water parcel (by respiration) is accompanied by the addition of phosphate and a lowering of the carbonate ion content. Thus an in situ increase in the balance of respiration over ventilation in deep waters, or an increase in the admixing of nutrient- and carbon-enriched water, should be reflected in the geological record by decreases in $\delta^{13}C$ relative to mean deep water, by increases in Cd/Ca (a proxy for phosphate), and by increases in sedimentary $CaCO_3$ dissolution.

An unresolved issue, discussed further in section 6.5, is the apparent disagreement between Cd/Ca and $\delta^{13}C$ indicators in the Southern Ocean [Boyle, 1990, 1992; Charles and Fairbanks, 1992]. We note this problem as a caveat to the interpretation, made in section 6.5, that carbon is trapped in deep water of the Southern Ocean during certain phases of each glaciation cycle. This interpretation is based on $\delta^{13}C$ gradients between the Antarctic and the equatorial Pacific (variable 20). In the absence of evidence to explain mismatches between cadmium and carbon indicators, we choose to interpret the $\Delta\delta^{13}C$ at face value and leave resolution of this apparent conflict to future work.

5. RESULTS

5.1. *Time Series Patterns*

Records of the past 150 kyr show a fundamental asymmetry in the way the system as a whole moves toward interglacial (positive) and glacial (negative) extremes (Figure 6). Widespread, positive transitions at glacial Terminations I and II, lead rapidly to conditions that are generally near full interglacial values during Stages 1 and 5e [Broecker and Denton, 1989]. This synchronous pattern fits the two-state model of Figures 2a and 4 (top). But negative transitions exhibit two distinct patterns. Variables 19, 18, 7, and 8 move significantly toward negative values near the end of Stage 5e [Belanger, 1982], yielding "short interglacials." This is the pattern which has been shown to characterize deep-temperature history in the Pacific and Indian oceans [Labeyrie et al., 1987; Shackleton, 1987; Broecker and Denton, 1989]. In contrast, the global $\delta^{18}O$ index and variables 17, 5, 14, and 16 have "long interglacials" which end at Stage 4. This pattern of progressive transitions fits the four-state model of Figure 2c. In spectral analysis, the "short" and "long" patterns will appear as early and late phases of the 100-kyr cycle, with the phase of variable 20 occupying an intermediate position. Thus the phase of this cycle expresses a fundamental aspect of the system's response, which we emphasize in this figure by ordering the time series according to the phase of their response at 100 kyr (Table 2). Whether the same or a different phase sequence occurs in the 23- and 41-kyr cycles is a question we will address later by formal spectral analysis.

Several conclusions can be drawn from the array of long time series shown in Figure 7.

1. Patterns of change are very different in different parts of the climate system. To some extent these contrasting patterns reflect different sampling rates or the application of smoothing procedures (variables 2, 3, 14, 20). But the fundamental character of the climatic response in the time domain varies markedly from one place to another.

2. As in Figure 6, many records displayed here exhibit abrupt, large-amplitude changes at the ends of glacial Stages 2, 6, 8, and 10 (Terminations I, II, III, and IV). The most rapid shifts occur in the surface ocean where a front oscillates over the coring site (e.g., variables 5, 7).

3. All time series from continental sites exhibit the "late, long-interglacial" pattern identified in Figure 6. This is also true of ocean sites where it appears that winds, steered by the northern hemisphere ice sheets, exert a strong control on the position of the polar front and the temperature of surface waters [Keffer et al., 1988] (variable 5), and thereby on the ventilation of intermediate (variable 12) and deeper (variables 14, 16) waters. However, several records exhibit the quite different "early, short-interglacial" pattern: Southern Ocean SST (variable 7), two of the $\delta^{13}C$ records that reflect the partitioning of carbon among ocean reservoirs (variables 8, 9), and the Vostok record of atmospheric CO_2. Many records appear too complex to fit neatly into this twofold, early-late grouping, first recognized by Belanger [1982]. But analysis in the frequency domain, discussed in section 5.3, shows that the same "early" and "late" responses characterize all three major cycles.

4. Major changes in our indicators of the $CaCO_3$ chemistry of intermediate and deep waters are ~180° out of phase. Dissolution in Atlantic intermediate waters (variable 12) is in phase with preservation in Southern Ocean deep water (variable 13), the latter being associated with NADW ventilation (variable 14). To the extent that a reduction in NADW flux is linked in time with the vertical fractionation of nutrients and carbon, this pattern is the expression in time series form of the process identified by Boyle [1988] and used by him to explain part of the glacial drawdown of atmospheric CO_2. In short time series, this process is seen as an event characterizing the ocean's most recent transition from a glacial to an

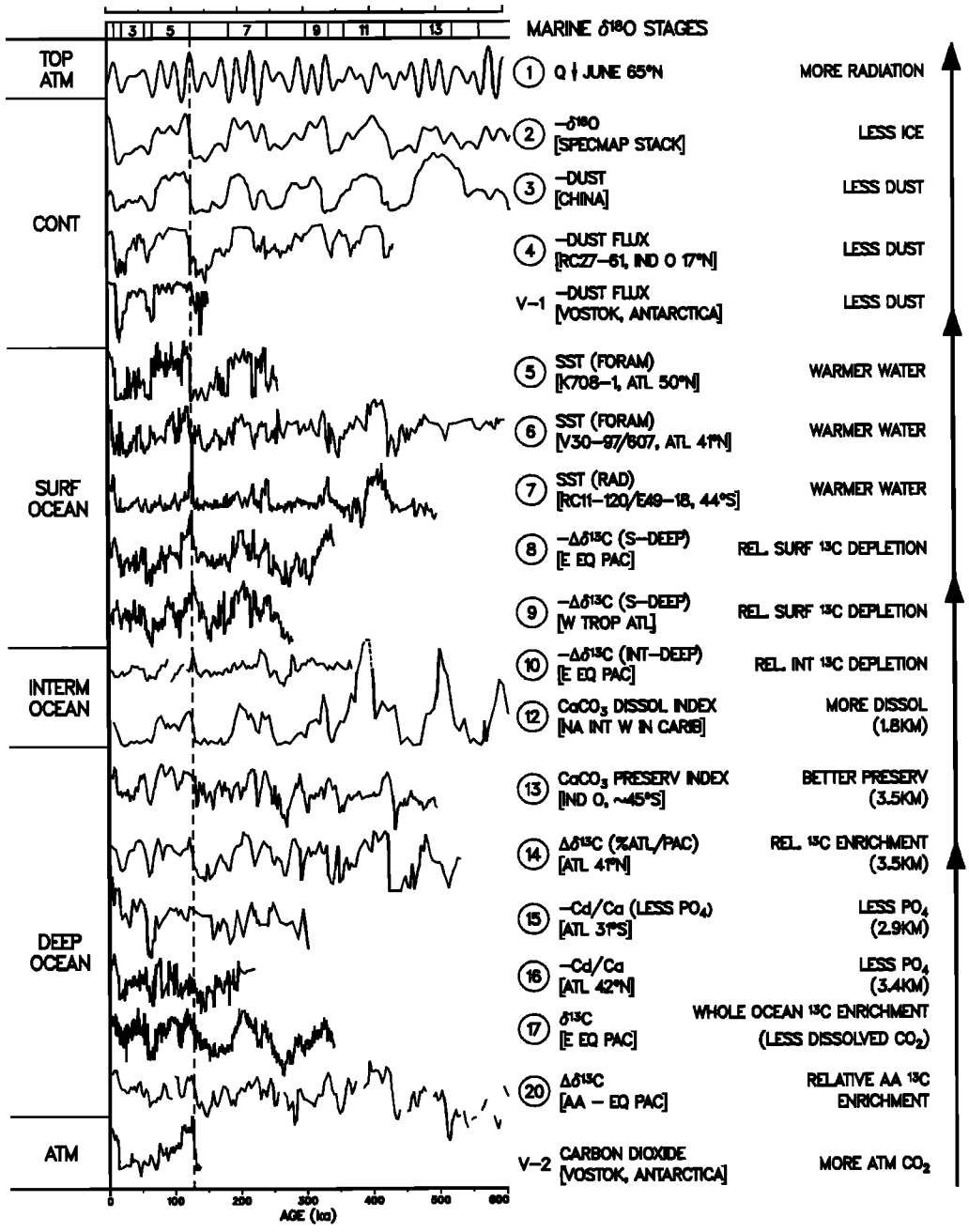

Fig. 7. Late Quaternary patterns of climate change. The observations are grouped by their location in the climate system. Scale factors for time series involving ^{13}C are the same for variables 8, 9, 10, 17, and 20; for other variables the factors are adjusted arbitrarily so that the range of each variable over the past 150 kyr is approximately the same. Plotting conventions as in Figure 6, documentation in Table 1. With three exceptions (variables V-1, V-2, and 3), the chronology of each time series is fixed by $\delta^{18}O$ stratigraphy (Figure 5). Note that all time series from continental sites exhibit the "long interglacial" pattern identified in Figure 6. This is also true of ocean sites where winds, steered by the ice sheets, exert a strong control on surface (variable 5) and subsurface (variables 14, 16) waters. Several records exhibit a clear "short interglacial" pattern: Southern Ocean SST (variable 7), two of the $\delta^{13}C$ records that reflect the partitioning of carbon among ocean reservoirs (variables 8, 9), and the Vostok record of atmospheric CO_2. The chronology of the two records from Vostok (V-1, V-2) is that suggested by correlations of dust [Petit et al., 1990] and air-$\delta^{18}O$ [Sowers et al., 1991] with marine $\delta^{18}O$ records. The chronology for variable 3 is independent of the marine $\delta^{18}O$ record and not tuned to astronomical time series [Kukla et al., 1990].

interglacial state [Boyle and Keigwin, 1987; Charles and Fairbanks, 1992].

5. Three time series that record conditions in deep water over the past 500 kyr (variables 13, 14, 20) display a systematic, essentially linear trend implying better ventilation and larger NADW flux over time. This is consistent with the trend in our longest record of Cd/Ca (variable 15). These trends are clear evidence that the system is not stationary in a statistical sense but, on the contrary, is slowly evolving — possibly toward a regime in which the response to orbital forcing would be quite different from anything captured in our data.

5.2. *Spectra of Climate and Radiation*

Viewed as time series, our observations on climate display complex patterns. But when examined in the frequency domain at an appropriate bandwidth, our data reveal a simple pattern in which every climate spectrum is dominated by variance in three fairly narrow bands centered near 23, 41, and 100 kyr (Figure 8). With the exception of the 23-kyr cycle in variable 10, every local record of climate is strongly coherent with $\delta^{18}O$ in all three major cycles (Table 2).

The radiation spectrum (variable 1) has power in the 23- and 41-kyr bands but virtually no power in the 100-kyr band. However, the spectrum of the radiation envelope has a peak at ~100 kyr, due to eccentricity. (There are also peaks at ~54 and ~35 kyr, due to the beating of obliquity against the two main precession frequencies.) In a later paper we will draw upon the relationship between climate and the envelope of the radiation curve to help account for the phasing of the 100-kyr cycles that dominate all climate spectra examined in this paper.

5.3. *Time-Space Structure of the Major Cycles*

Our main objective in constructing an array of time series is to determine the temporal and spatial structure of the Milankovitch cycles. Fourteen records are long enough to treat statistically, yielding a total of $3 \times 14 = 42$ responses to be investigated (Table 2). We need to know three things: (1) are the responses at different sites synchronous within each cycle? (2) are they mutually coherent; i.e., are they linearly correlated at a given frequency when corrected for phase differences? (3) if the responses are not synchronous, what is the spatial pattern of the progression within each cycle?

A definitive answer to the first question is given by calculating the cross spectrum of each local response against $\delta^{18}O$. The responses are not synchronous (Table 2). In the 23-kyr cycle, the total range of phases is 111° (~7 kyr); in the 41 kyr cycle, 73° (~8 kyr); and in the 100-kyr cycle, 96° (~27 kyr). A partial answer to the second question is given by the same set of cross spectra. With one exception (the 23-kyr response of variable 10), all local responses are coherent with $\delta^{18}O$. Because the local responses might well be coherent with $\delta^{18}O$ but not with each other, we should also examine the entire 14×14 matrix of cross spectra. But rather than stretching the reader's patience with this cumbersome numerical exercise, we prefer to filter each time series and obtain an answer by simply looking at the amplitudes of individual oscillations as they vary over time. Results for the 23- and 41-kyr cycles are shown in Figure 9. Our filters use a convolution algorithm that averages information over a sliding 100-kyr interval. At this resolution, each cycle appears as a mutually coherent set of waves that progress through the system — a pattern that is a striking contrast to the standing-wave pattern we purposely forced on $\delta^{18}O$ signals in the same cores (Figure 5). The display in Figure 9 also demonstrates that conclusions drawn from the mean phases reported in Table 2 do not hide significant irregularities. In a later paper we will show that this is also true of the 100-kyr cycle.

Having demonstrated that the Milankovitch responses progress through the system in an orderly way, we now ask what the geographic pattern of the phase progression in each cycle is and if this pattern differs from one cycle to another. After eliminating variable 10, owing to its incoherent response in the 23-kyr band, a total of 13 variables remain to be considered. Because variations around the calculated mean phases are quite large, it would be unwise to attribute too much significance to the details of any sequence. Instead, we ask "Which system responses occur in essentially the same sequence in all three cycles?" The surprisingly simple answer is that, with the exception of variables measured at two sites, the main features of the geographic progression are the same in the three cycles (Figure 10). The two exceptions are variables that exhibit a phase in one cycle that is very different from the phase exhibited in the other two cycles. Variable 13 ($CaCO_3$ preservation at 41°S) responds early in the 41-kyr cycle and late in the other cycles. As discovered by Ruddiman and McIntyre [1981], variable 6 (SST at 41°N) responds much later in the 23-kyr cycle than in the other cycles.

In order to focus attention on the main pattern revealed by our data, we will set aside the responses of variables 13 and 6 as anomalies that are more appropriately investigated elsewhere. Then a statistical argument can be made that the responses of the other 11 variables occur in two discrete clusters within each cycle (Table 2). We will refer to these clusters as an early and a late group of responses (Figure 10). In time, the early group leads $\delta^{18}O$, and the late group is on phase with or slightly lags $\delta^{18}O$. In space, the early responses occur in deep waters of the South Atlantic (variable 15) and Antarctic (variable 20) oceans, and in surface waters of the Antarctic (variable 7) and tropical oceans (variables 8, 9); whereas the late responses occur on land (variables

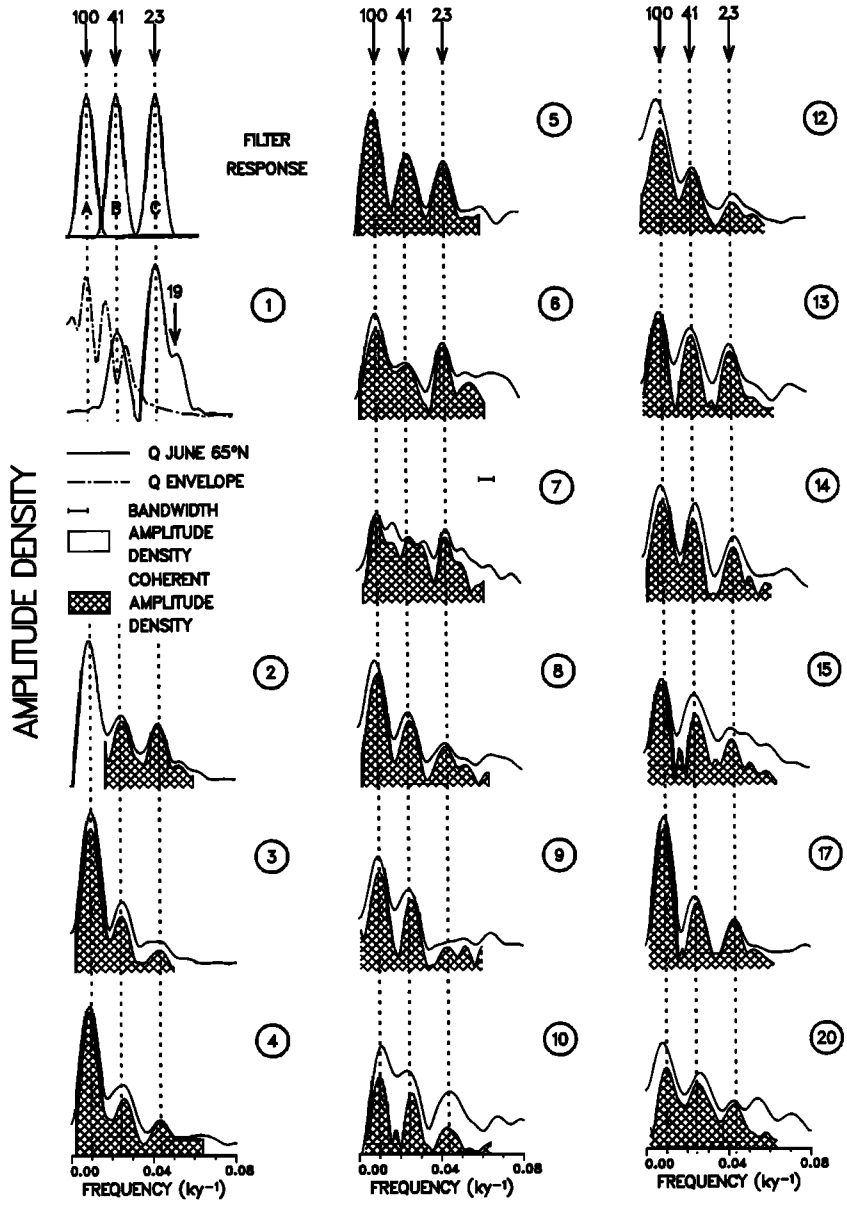

Fig. 8. Amplitude-density spectra of 20 long climatic time series (400 ka ≥ t > 0 ka). All records are dominated by variation in bands centered at periods near 100, 41, and 23 kyr. Solid lines in panels 1-20 are spectra of total amplitude, calculated from variance-density spectra. For $\delta^{18}O$ (variable 2), the patterned area shows the fraction that is coherent with radiation (variable 1); for other variables, the patterned area shows the fraction coherent with $\delta^{18}O$. Dashed-dotted line (in panel 1) is the spectrum of the envelope of the radiation curve. Curves B and C (top left) are the frequency-response functions of band-pass filters used in Figure 9.

3, 4, 17), at a range of depths in the open boreal ocean (variables 5, 14), and in low-latitude intermediate waters (as shown by an index of CO_3 dissolution, variable 12). A 1.2 million-year $\Delta\delta^{13}C$ record of Atlantic intermediate water confirms this late-response pattern for the 41- and 100-kyr cycles [deMenocal et al., 1992], but in the 23-kyr band the $\Delta\delta^{13}C$ response has a small amplitude and is not coherent with $\delta^{18}O$.

The very late phase of the 23-kyr SST response of variable 6 seems anomalous in the context of this paper. However, we emphasize that this "lagging warmth" pattern must be climatically important because it can be mapped over a quadrant of the northeast Atlantic that extends from 54°N to 18°N and as far west as 21°W [Imbrie et al., 1989]. Yet none of the explanations proposed to date is very satisfactory, including one that relates the response to the first

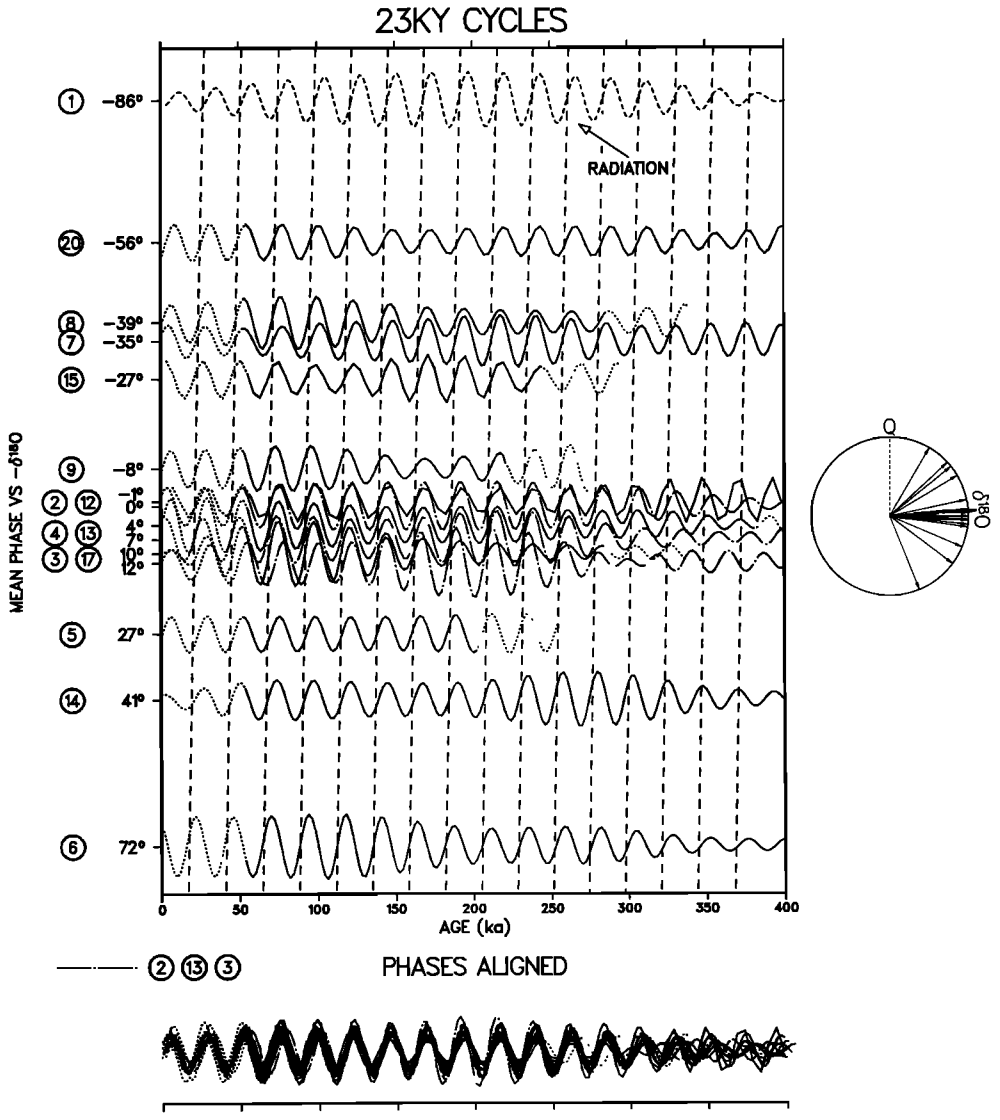

Fig. 9a. The 23-kyr climate cycles. The 23-kyr component of each time series is extracted with the bandpass filter described in Figure 8, normalized, and placed on the y axis according to the mean phase difference (°) with respect to $\delta^{18}O$ (variable 2). Lines drawn with a slope of 360°/23 kyr show that the local climatic responses to radiation progress systematically through the system with respect to the local changes in $\delta^{18}O$ that are used to align the records (Figure 5). When phase-aligned and superposed (bottom panel), this progressive wave is seen to be coherent with the forcing (Table 2). Dotted curves mark intervals where 10% or more of the cyclic convolution integral is based on extrapolated data. In the phase wheel (right), climate variables are plotted with respect to the maximum June radiation at 65°N (Q).

derivative of the ice-volume curve [Ruddiman and McIntyre, 1984]. In this view, the maximum meltwater production that occurs 90° (one-quarter cycle) after the maximum ice volume leads to an oceanic cooling; and the minimum in melting that occurs 90° after the ice minimum leads to a warming. Since the ice minimum itself occurs nearly 90° after the radiative forcing, the result would be an SST signal that is out of phase with the radiative forcing by nearly 180° (one-half cycle). However, it is by no means clear why the effect would occur in the 23-kyr band and not in the 41- and 100-kyr bands where the magnitude of changes in meltwater input must be considerably greater.

Later in this paper (section 6.6) we examine the phases of initial, early, and late responses of the system to determine the combination of latitude and season where the system is most sensitive to the ra-

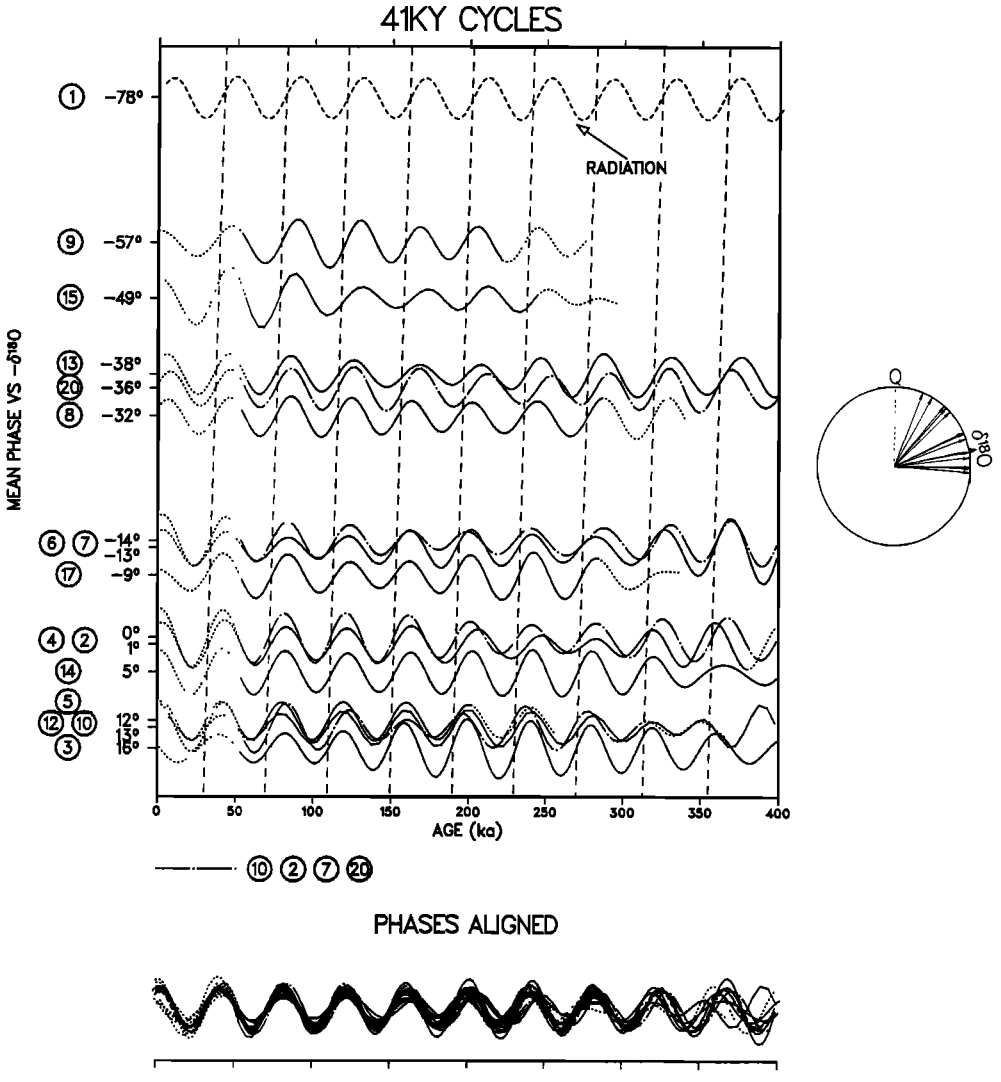

Fig. 9b. The 41-kyr climate cycles. The 41-kyr component of each time series is extracted with the band-pass filter described in Figure 8, normalized, and placed on the y axis according to the mean phase difference (degrees) with respect to $\delta^{18}O$ (variable 2). Dashed lines have a slope of 360°/41 kyr. Other features as in Figure 9a.

diative forcing. We conclude that the radiative forcing is best represented by the insolation curve for June 1 (rather than mid-June) for high latitudes in the northern hemisphere. In the 23-kyr band the phase of this curve is within a few degrees of being exactly out of phase with variable 6. This raises the interesting possibility that the warm SST response of variable 6, which seems anomalous in its phase, might actually represent the initial, essentially unlagged response of the atmosphere and surface ocean to a radiation minimum. Why this response would involve the warming of surface waters at this site is a problem that clearly deserves more study.

5.4. *Summary*

We conclude that the 23- and 41-kyr cycles are linear responses to Milankovitch forcings which exhibit essentially the same two-step pattern in time and space. The early responses we see in long time series are changes in the properties of surface and deep waters of the southern hemisphere, and in the properties of surface waters of the equatorial ocean. Later responses occur in the northern hemisphere — on land and at a range of depths in the boreal Atlantic. In the next section, we show that the initial responses to the orbital forcing must be earlier than

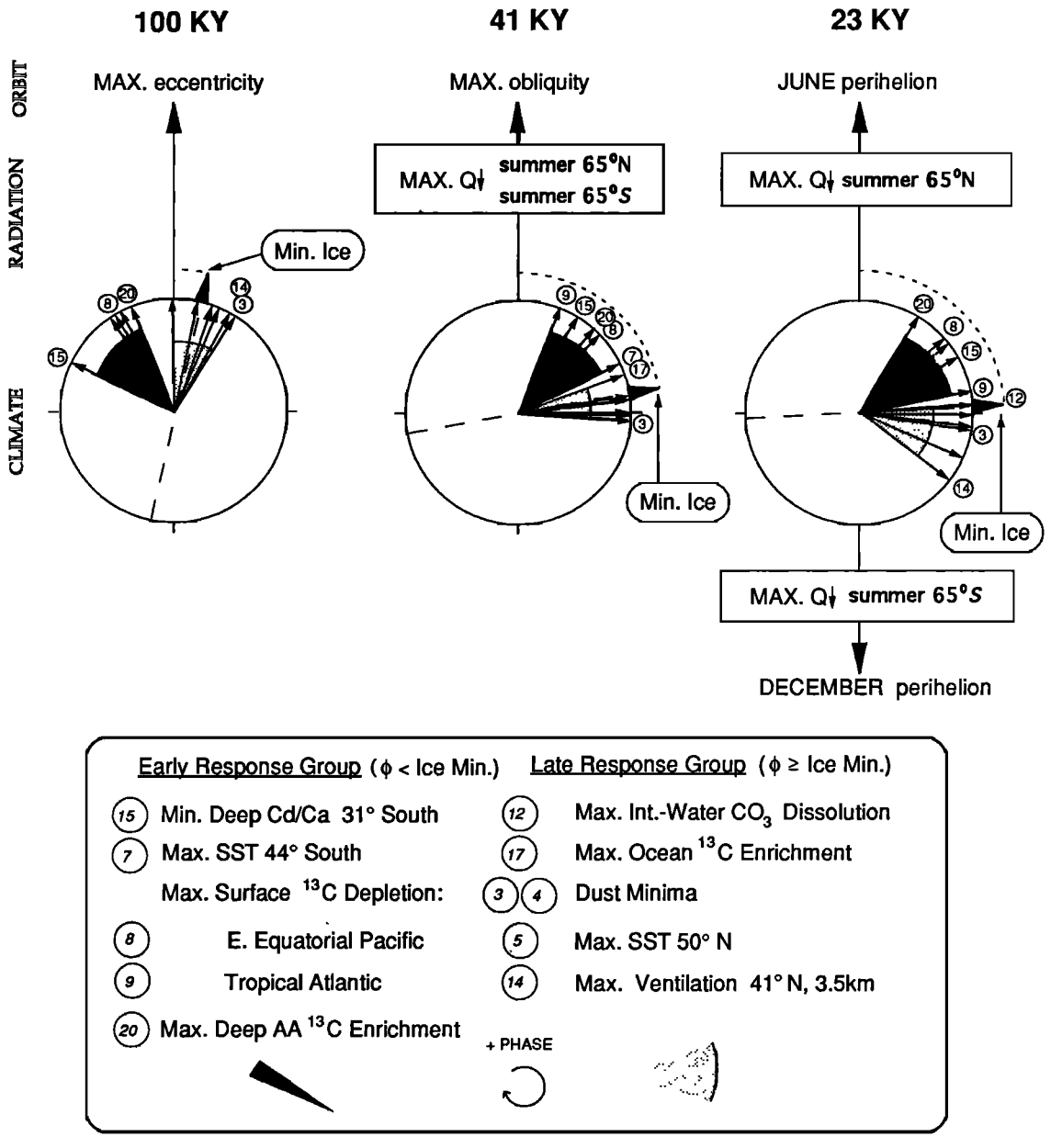

Fig. 10. Phases of orbital, radiation, and climatic cycles. Phases of the 11 climatic variables that are coherent with $\delta^{18}O$ are plotted as short vectors. These fall into two groups; in each group the progression of responses is statistically the same in all three cycles (Table 2). An early group of responses precedes ice volume. A late group is on phase with or slightly lags ice volume. We draw an important conclusion from the phase of the early responses in the 23-kyr and 41-kyr cycles with respect to the latitudinal pattern of radiation. The initial response to this forcing — although not recorded in these data — must occur at high latitudes in the northern hemisphere. Phase wheel zeros are arbitrarily set to the maximum of the 100-kyr eccentricity cycle, the maximum of the 41-kyr obliquity cycle, and June perihelion in the 23-kyr precession index cycle. The dashed vector in each phase wheel records the mean phase of the ice volume ($\delta^{18}O$) cycle with respect to these zeros. Solid vectors in each wheel show the mean phase of other climate variables as measured with respect to $\delta^{18}O$. Vectors labeled with boxes show the phase of maximum summer radiation at two latitudes. The winter radiation maximum (not shown) is exactly out of phase with the summer maximum.

any we observe in our array of long time series. We deduce that these must occur in the Arctic and support this deduction with observations in short time series. We then use the entire spatial progression of responses — initial, early, and late — to identify causal pathways. These ideas are organized as a simple conceptual model of processes that operate in the atmosphere and ocean along prescribed pathways.

6. A MODEL OF THE GOVERNING PROCESSES

Our first step in developing this model is to show that at least four end-member states are needed to record the system's evolution (section 6.1). In section 6.2, we obtain insights into the way the ocean is ventilated at two of these states (glacial and interglacial) by examining vertical sections measured in the modern ocean and reconstructed for the LGM. In sections 6.3 and 6.4, we consider where the initial response to orbital forcing must occur. In section 6.5, we use the spatial progression of responses that follow the initial response, combined with insights gained from comparing the modern and LGM oceans, to reconstruct two other states (preglacial and deglacial); and we identify causal pathways along which the initial response is propagated through the system. In section 6.6, we postulate sources of inertia to explain the temporal clustering of responses along these pathways. In a quantitative system model, these sources appear as the inertial parameters of four discrete subsystems.

6.1. *Degrees of Freedom*

How many degrees of freedom does the system have at each Milankovitch frequency? A first-order dynamic model provides the theoretical basis for making an estimate (Figure 2). Our analysis of long time series shows that the system's responses are distributed in two phase-clusters (Figure 10), from which we conclude that four end-member states (interglacial, preglacial, glacial, and deglacial) are the minimum needed to describe adequately the system's evolution.

6.2. *Glacial and Interglacial States Compared*

To obtain insights about ocean circulation in a glacial state, we compare a vertical section of the modern western Atlantic (Figure 1b) with a section reconstructed for the eastern Atlantic at the LGM (Figure 1c) by Duplessy et al. [1988] and recontoured by Broecker [1989]. These figures are a compilation of observations previously published and widely discussed. Because $\delta^{13}C$ in the glacial ocean was on average about 0.4‰ more negative than today, isopleths emphasized by shading are shifted in the glacial reconstruction by 0.4‰. Evidently, the processes that ventilate the glacial Atlantic were very different from those that ventilate the modern ocean. Today, the Atlantic is mainly ventilated by NADW which is formed partly by deep overflow from the Nordic Sea and partly by wintertime convection to intermediate depths in the Labrador Sea, with a small contribution of Mediterranean Water [McCartney and Talley, 1982, 1984]. At the LGM, a weakening of the overflows apparently allowed a northward penetration of nutrient-enriched Southern Ocean Water (SOW). Ventilation from North Atlantic sources was limited mainly to intermediate depths. By analogy with convective processes operating in the wintertime Labrador Sea today, we infer that this ventilation pattern is the open ocean's convective response to a wind field steered by the great ice sheets and bringing cold, dry air over a wide expanse of the open boreal Atlantic.

6.3. *The Milankovitch Link*

Where does the glaciation process begin? Theoretical analysis of this problem began with the work of Milankovitch [1930], who concluded that the initial response to orbital forcing must occur in the high latitudes of the northern hemisphere in summer, ice sheets being initiated there whenever summer melting fails to remove the winter snow. More recent glaciological investigations have generally confirmed this idea [Kukla et al., 1981; Budd and Rayner, 1990], which is also supported by experiments with numerical models that resolve regional components of the seasonal energy budget [Short et al., 1991].

Theories pointing to northern hemisphere summer as the driver of the glaciation process find strong empirical support in the phase observations summarized in Figure 10. This support depends on examining the phase relationships in the precession and obliquity bands simultaneously. For example, if information were available only in the 41-kyr band, the phase evidence by itself would point unambiguously to summer as the critical season but would suggest that the southern hemisphere is the critical place. This is because the group of early responses includes three (variables 7, 15, 20) from the southern hemisphere, and none from the northern hemisphere, that lag behind the southern summer radiation curve by less than 90°. A lag of this magnitude is easily explained as the response of a system (the ice sheets) that on theoretical grounds are known to have a time constant on the order of 10 to 20 kyr [Weertman, 1964].

If we accept this evidence from the 41-kyr band that summer is the critical season, the phase evidence in Figure 10 for the 23-kyr band indicates that the northern hemisphere must be the critical place. This is because a southern summer forcing would imply an unreasonable lag of nearly 270°. Even with an infinite time constant, the lag of a linear,

single-exponential system without delay is only 90° [Jenkins and Watts, 1968]. Thus the hypothesis of southern summer forcing in this band would require an initial delay of 11.5 kyr (180°) before the effect of the ice-sheet time constant began to be felt. From a physical point of view, this seems highly unlikely.

Thus both theory and observation indicate that the initial response to orbital forcing must occur at high latitudes in the northern hemisphere. Why, then, is direct evidence of this response not seen in our long time series? Our answer is that the initial response must occur in or near a part of the ocean where we have no long records, namely the Arctic Ocean and Nordic Sea (Figure 11). To explain the early southern hemisphere response we postulate that the initial response is transmitted rapidly to the Southern Ocean by North Atlantic Deep Water. This is the basic mechanism proposed by Weyl [1968] and used by Imbrie et al. [1989] to explain their more detailed pattern of SST responses. To explain the early equatorial response, we postulate that the early response in the southern hemisphere drives a change in the production of Subantarctic mode waters which ventilate thermocline waters all the way to the equator.

It has long been known that the rate of thermohaline overturning is very sensitive to changes in surface salinity at the sites where deep water is formed [Worthington, 1976]. Since Weyl's classic application of this principle to the ice age problem, the idea has figured in many climate theories. Our application emphasizes recent oceanographic studies of the Arctic Ocean and the Nordic Sea [Swift and Aagaard, 1981; Aagaard et al., 1985; Aagaard and Carmack, 1989; Mysak et al., 1990] . These studies imply that small changes in the freshwater budget of the Iceland gyre, for example, would strongly influence the rate at which dense water forms by winter convection and then overflows the Denmark Strait to ventilate the deep Atlantic (Figure 11). Geological

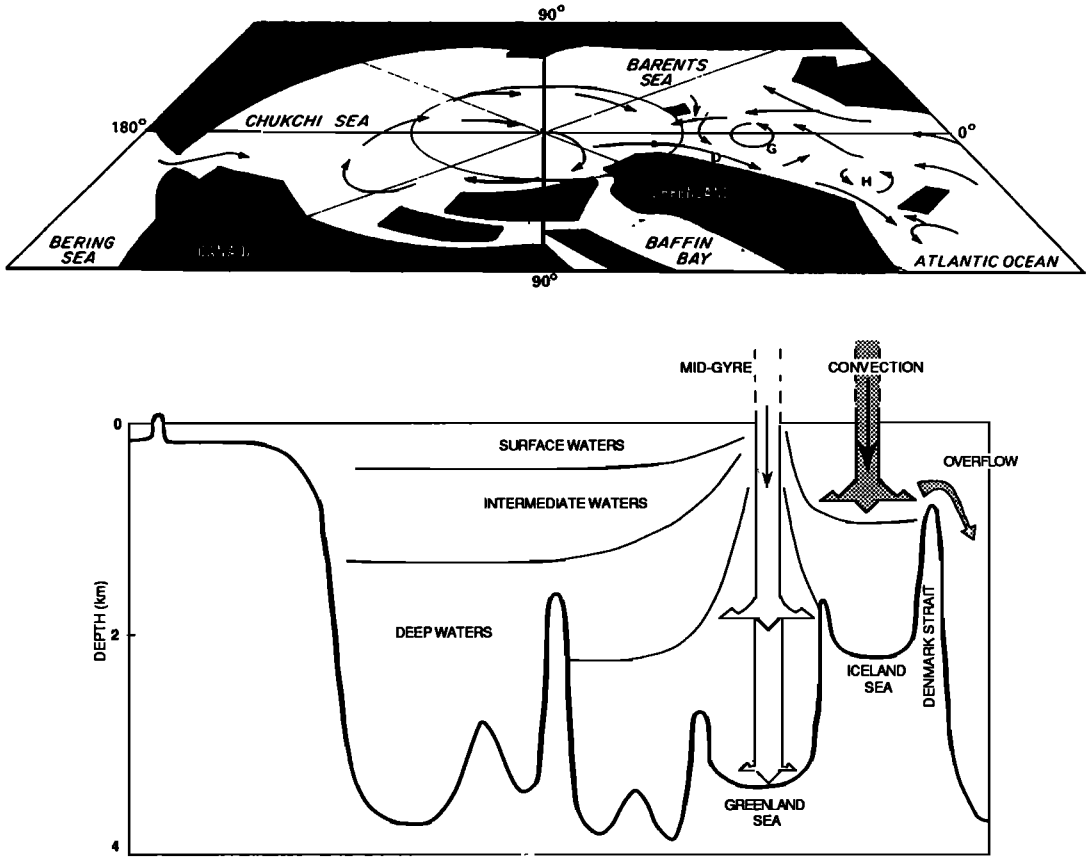

Fig. 11. Schematic circulation and water mass structure in the Arctic Ocean and adjacent Nordic Sea [Aagaard et al., 1985]. The deep North Atlantic is ventilated by water that forms by winter convection in the Iceland gyre, sinks to intermediate depth, and overflows the Denmark Strait. Here we suggest that orbitally forced changes in the salinity of this gyre modulate the overflow. Today, freshwater which exits the Arctic Ocean in the East Greenland current (D) passes close to the Greenland (G) and Iceland (H) gyres. A change in the P-E or sea ice contribution to this flow is one possible modulating mechanism.

evidence that times of lower salinity in the Nordic Sea are in fact associated with reduced thermohaline circulation confirms the importance of these marginal seas as regulators of the thermohaline circulation [Veum et al., 1992].

Two terms in the freshwater budget of the Iceland Sea, the import of Arctic sea ice in the East Greenland current and precipitation minus evaporation (P-E), have particular interest here because they suggest a physically reasonable link to the Milankovitch forcing. Recent experiments with a steady-state, general-circulation model coupled to a 50-m mixed layer have investigated these links. These experiments demonstrate that the response of this model to an orbital forcing is to change the thickness of sea ice in the Arctic Ocean and to alter P-E north of the Arctic Circle. In one published study, a control experiment with modern radiation was compared with an experiment in which the incoming radiation was prescribed for 9000 years ago (9 ka) — a time when both the precession and obliquity terms contributed to an increase in northern hemisphere summer radiation [Kutzbach and Gallimore, 1988]. Other boundary conditions were held constant. When compared with the 9 ka experiment, the control experiment with less radiation shows a decrease in boreal temperatures, an increase in P-E north of 45°N owing to reduced evaporation, and an increase in sea ice.

Unpublished experiments with the same model, in which summer radiation was decreased still further by setting the obliquity at 22°, perihelion at December, and eccentricity at 0.04, show even larger decreases in temperature and larger increases in P-E and sea ice. In these experiments the atmospheric responses were clearly concentrated north of the Arctic Circle. The increase in annual P-E as the simulated climate changes from conditions of maximum to minimum summer radiation is approximately 10%. This increase stems primarily from reduced evaporation. The corresponding annual temperature decrease is about 5°C and the thickness of sea ice approximately doubles. Over the land bordering the Arctic Ocean, there is also an increase in P-E and in freshwater runoff to the ocean. These simulations of high-latitude climates with present-day climate models are not very accurate and it will be important to repeat these kinds of orbital sensitivity experiments as models are improved.

6.4. *Records From the Nordic Sea*

Thus a key prediction of our conceptual model of the glaciation process is that the initial response to Milankovitch forcing is a change in the intensity of winter convection in the Iceland gyre. The challenge that remains is to test this prediction against long time series from the Nordic Sea. As discussed in this section, technical problems with dating and interpreting long sedimentary records have so far made it impossible to provide a clear confirmation or rejection of this idea.

Quantitative investigations of coccoliths [Belanger, 1982; Bleil and Gard, 1989], forams [Kellogg et al., 1978; Belanger, 1982], and diatoms [Karpuz and Schrader, 1990] show clear biotic gradients across the Nordic Sea just north of Iceland, and provide clear evidence that the oceanographic history of the Iceland Sea over recent glaciation cycles has been very different from that of the Norwegian Sea. In addition, there is evidence that elements of the zooplankton community that thrive today in subpolar waters of the open North Atlantic (including the foram *Globigerina bulloides*) behave very differently from the phytoplanktonic coccoliths. In the Norwegian Sea, for example, the *bulloides* assemblage is abundant only during Stages 5e and 1, yielding a "short Stage 5" pattern, whereas the coccoliths have roughly equal abundance peaks during all three Stage 5 interglacial substages (Figure 6). One ecological explanation of this foram-coccolith difference is that coccoliths can bloom in response to shallow convection in a thin layer above the summer thermocline, an environment apparently unsuited to *G. bulloides*. This reading of the data would provide support for our prediction, namely that convection to intermediate depths in the Iceland gyre ceased early in Stage 5.

To pursue the matter further, we require not only a more accurate chronology of events, but information about the flux of biotic and sedimentary components that such a chronology would yield [Veum et al., 1992]. In the absence of a refined chronology and stratigraphy therefore, we can say only that the data in hand do not contradict the prediction and that one plausible interpretation of the data in hand provides slender support.

As a substitute for long sedimentary records, we have compiled a set of ^{14}C-dated time series that allow us to examine selected elements of the system's response over the past 25 kyr at high northern and southern latitudes. One of these time series is from a core in the northern Greenland Sea (Figure 12). The location of this core, and the fact that each of 22 $\delta^{18}O$ measurements is dated by accelerator mass spectrometry (AMS) of ^{14}C, make it the focal point of our analysis of the deglaciation process. A striking feature is the spike of light isotopic values centered at ~14.5 ka [Jones and Keigwin, 1988; Jones, 1991]. Considering the core's location, the spike can reasonably be interpreted as a flooding of meltwater into this marginal sea. Geologists familiar with the region see this meltwater event as evidence of a rapid decay of an ice sheet occupying the continental shelf of the Barents Sea [Jones and Keigwin, 1988], and perhaps other shelves in the region [Lehman et al., 1991].

In Figure 13 we place this early Nordic deglaciation event (d) in a broader context. This includes a

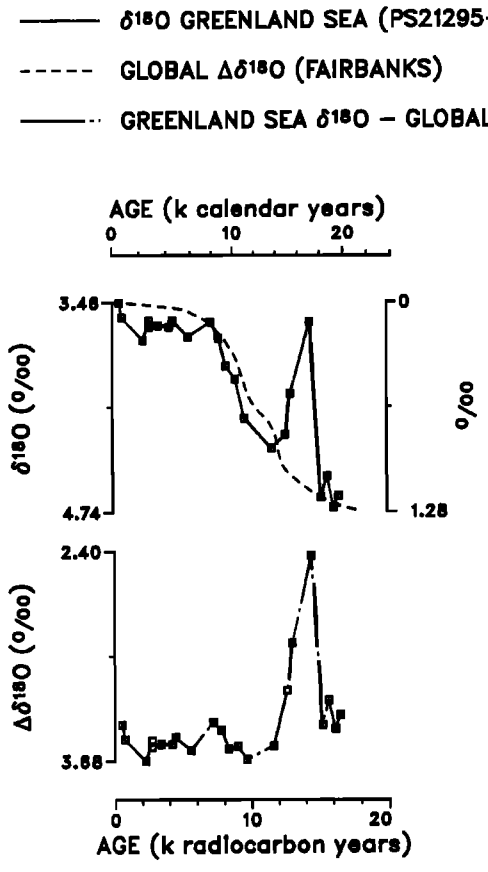

Fig. 12. Marine record of an early Nordic deglaciation event in the northern Greenland Sea [Jones and Keigwin, 1988; Jones, 1991]. The $\delta^{18}O$ composition of planktonic forams in AMS ^{14}C-dated core PS21295-4 indicates that isotopically light meltwaters flooded the Nordic Sea 15,200 radiocarbon years ago. This event is interpreted as the rapid decay of an ice sheet occupying the continental shelf of the Barents Sea (and perhaps other shelves in the region). The time scale in calendar years is a calibration provided by E. Bard and is based mainly on data in Bard et al. [1990a].

record of fluctuations along the southern margin of the Laurentide ice sheet (b), a record of global sea level (c), and a record of SST at 55°S (e). To compare these climatic responses with a radiation curve for 65°N, it is necessary to convert the ^{14}C-based chronologies to calendar years [Bard et al., 1990a; Stuiver et al., 1991]. Taken together, this sequence of changes during the last deglaciation supports (but surely cannot be taken to prove) the main conclusion we deduced earlier, namely, that the initial response to orbital forcing occurs in the northern hemisphere, involves the Nordic Sea, and is transmitted rapidly to the Southern Ocean [Lehman et al., 1991]. To obtain more detailed information about the role of the Nordic Sea in the deglaciation process, we need other records. These we will examine in a later paper as part of our investigation of the 100-kyr cycle.

6.5. *Process Model*

We now describe a chain of mechanisms by which the initial responses of the ocean and atmosphere in the Arctic might be propagated throughout the climate system along pathways identified in Figure 3. These responses arrive at different places at different times because sources of inertia that control the flow of climatic energy along these pathways differ from one mechanism to another. To see how the system as a whole progresses through a generic Milankovitch cycle, we provide a synoptic view of the responses at four end-member states. The varying intensity of different responses is suggested by symbols showing the size of the northern ice sheet, the extent of sea ice in both hemispheres, the presence of marine-based ice sheets, the position of maximum westerlies in both hemispheres, the export flux of NADW, and recirculation fluxes in the boreal Atlantic and Antarctic oceans.

This diagram has three significant limitations, quite apart from the geometric distortions that are inevitable in such a simplified view. First, by choosing to present the model in this generic form we are unable to show how the intensity of responses differs among cycles. In reality, the 23- and 41-kyr cycles involve only modest changes in ice volume and sea level as compared to the 100-kyr cycle. Thus marine-based ice sheets would form only at sea level lows associated with the larger cycle [Weertman, 1974; Grosswald, 1980; Hughes, 1987]. Second, we are unable to show how variations in the production of Subantarctic modewaters are linked to shifts in the wind field. Because these modewaters are important in ventilating the southern hemisphere thermocline today [McCartney, 1982; Toggweiler et al., 1989; Toggweiler et al., 1991], we infer that variations in their production are recorded as the enrichment or depletion of $\delta^{13}C$ in our time series of tropical plankton (Figure 3; variables 8, 9). Third, we do not illustrate changes in the atmosphere and on the continents that are closely linked to the extent of northern ice sheets [Manabe and Broccoli, 1985; COHMAP Members, 1988; Kukla et al., 1990].

6.5.1. *Interglacial state.* We start by examining the interglacial state and assume that the Holocene is a typical example of this condition. The northern ice sheets are now at their minima, restricted to Greenland and few small residual icecaps. Elsewhere on the continents, the climate is at its humid extreme (variables 3, 4) and the terrestrial biomass at its maximum (variable 17). The northern sea ice field is near its minimum extent, and the salinity of surface waters in the Nordic Sea is near its maximum.

The warm-to-cold-water conversion process which drives the global overturning circulation and

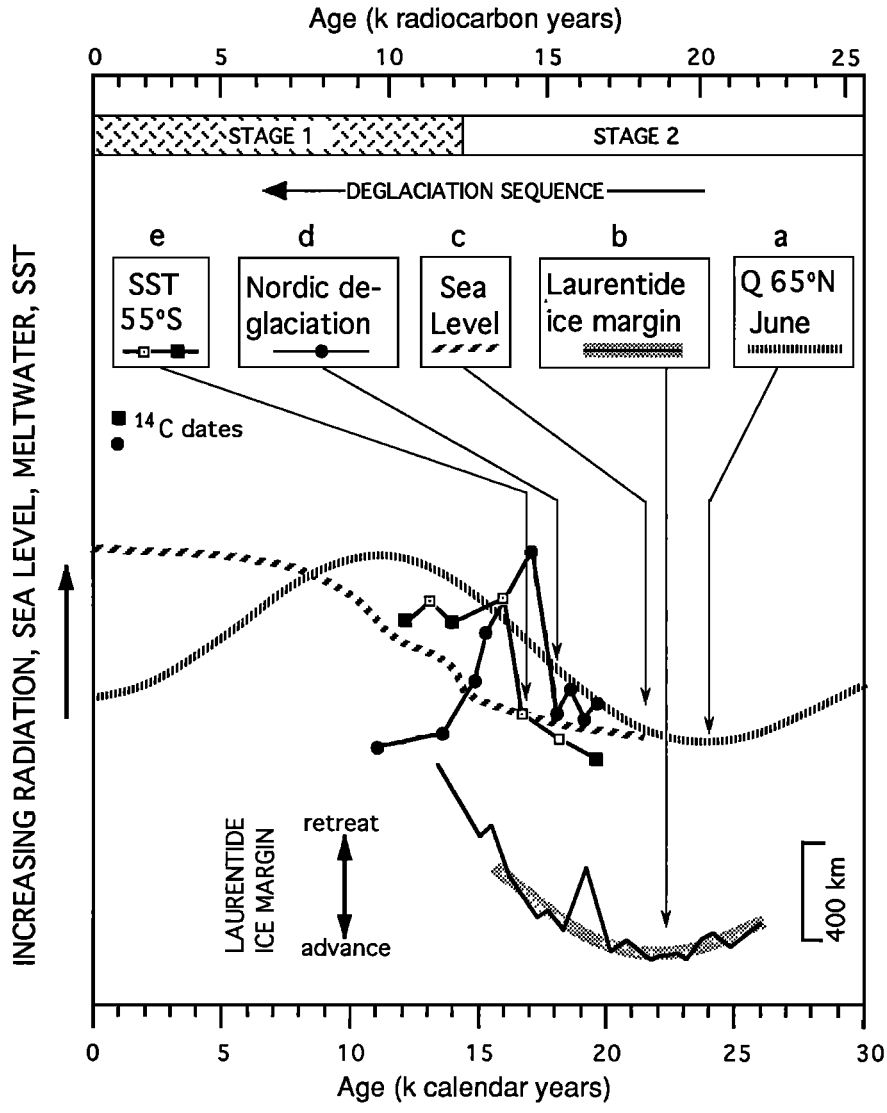

Fig. 13. Evidence that the initial response to orbital forcing is in the northern hemisphere. The sequence of changes recorded by curves a-e supports the conclusion (drawn from the phase sequence in Figure 10) that responses in the northern hemisphere initiate the deglaciation process. Arrows point to minima in radiation and sea level, a maximum in the ice margin, and step responses of the surface ocean. (a) Incoming June radiation at 65°N [Berger, 1978a]. (b) Position of the southern margin of the Laurentide ice sheet (Miami sublobe) shown as solid line [Broecker and Denton, 1989]. The stippled band shows the low-frequency trend of glacial maxima, which is delayed 1 or 2 kyr with respect to radiation. (c) Eustatic sea level record from Barbados corals [Fairbanks, 1989]. (d) $\Delta\delta^{18}O$ record of meltwater in the Greenland Sea [Jones, 1991]. (e) Diatom estimates of sea surface temperature in the Southern Ocean [Bard et al., 1990b]. The ^{14}C-based chronologies of curves b-e have been converted to calendar year chronologies using a calibration provided by E. Bard and based mainly on data in Bard et al. [1990a].

powers the North Atlantic heat pump has two main branches which we designate as the Nordic heat pump (overflows from the Nordic Sea) and the boreal heat pump (convection in the Labrador Sea). As noted previously, these elements in the global conveyor circulation [Broecker, 1990] have been referred to by Lehman and Keigwin [1992b] as the upper and lower belts. The NADW export-flux that results from these two mechanisms transports heat to the Southern Ocean [Reid and Lynn, 1971; Wunsch, 1984; Rintoul, 1991], with the Nordic pump transporting more heat than the boreal pump [Lehman and

Keigwin, 1992a, b]. This transport is sufficient to restrict the growth of southern hemisphere sea ice to its modern seasonal limit.

The sea ice field and the resulting latitudinal temperature gradient interact with the atmosphere and ocean to produce the modern pattern of winds, ocean fronts, and plankton communities. As discussed below, this wind pattern exerts a strong control on the circulation and water-mass chemistry of the ocean and thereby influences the concentration of CO_2 in the atmosphere. Wintertime convection near the position of the maximum westerlies produces "mode waters" that are recirculated within the subtropical gyres, ventilating the thermocline all the way to the equator [McCartney, 1982; Toggweiler et al., 1991].

6.5.2. *Preglacial state.* In response to a continuous decrease in summer radiation, the atmosphere and surface ocean in the Arctic region cool, evaporation decreases, and fields of snow and sea ice expand. Although ice sheets have now started to grow, the time constants of this process are so large that a significant response in terms of global ice volume and sea level will not be seen for many thousands of years.

The immediate and decisive consequence of the initial responses in the Arctic is a freshening of surface waters, first in the Iceland and Greenland seas, and later in the Norwegian Sea. This slows and eventually nearly shuts off the production of overflow waters which, by entraining warmer waters, had transported heat in significant quantities to the Southern Ocean in the deeper layers of NADW. The production of upper NADW that occurs in the Labrador Sea is unaffected. The system is now in a one-pump mode, with global overturning and the pumping of heat into the North Atlantic region at their minimum values. We also consider it likely that Antarctic sea ice and hence brine production would increase.

All these effects operate in concert to decrease the north-south buoyancy contrast and bring it toward a value characteristic of the preglacial state. This would imply a stronger northward flow of very deep and bottom waters of southern origin into the North Atlantic basin, thus pushing the mixing front between waters of northern and southern origin further northward [Stocker et al., 1992].

The cooling of subsurface waters in the polar regions of the Southern Ocean has dramatic consequences for the entire climate system. Observational and modeling studies show that the temperature immediately below the mixed layer is the critical factor in determining how much sea ice forms [Gordon and Huber, 1990; Martinson, 1990]. With cooler subsurface waters, the sea ice quickly expands to its maximum value. This condition increases the latitudinal temperature gradient. The resulting change in the wind field [Oglesby, 1990] shifts surface fronts, plankton communities, and water masses northward [Howard and Prell, 1992]. The system is now in a preglacial state. These early responses in the surface Antarctic (variable 7) are on phase and strongly coherent with a redistribution of nutrients among ocean reservoirs, as shown by our ^{13}C and Cd/Ca data from sites near the equator and in the southern hemisphere (variables 8, 9, 15, 20). The effect of this redistribution would be to drive down the level of CO_2 in the atmosphere and thus serve as a strong and early positive feedback on local processes already acting to enlarge the northern hemisphere ice sheets [Sundquist and Broecker, 1985; Boyle, 1988; Broecker and Peng, 1989].

Although it is not yet certain what mechanisms are responsible for these changes in ocean chemistry, available $\delta^{13}C$ data indicate that a mechanism operating in the Southern Ocean must be an independent driver of benthic $\delta^{13}C$. Curry et al. [1988] drew this inference from an array of short records showing that variations in $\delta^{13}C$ that occur in the deep Antarctic on ice age time scales cannot be explained as a result of a simple increase or decrease of NADW outflow. Our long $\Delta\delta^{13}C$ record (variable 20 in Figure 6) supports this important conclusion.

Today, the Atlantic outflow is cycled through the Antarctic, entering the Pacific mainly as Antarctic Bottom Water. Pacific ^{13}C levels are low because Pacific deep water is "downstream" from both the Atlantic and Antarctic. The transit of Atlantic outflow waters through the Southern Ocean is sufficiently fast that biological alterations and gas exchange effects are small. But during the preglacial (and glacial) states, we see a depletion of ^{13}C in Antarctic deep water which exceeds the depletion in Pacific deep water. Antarctic deep water that is so depleted in ^{13}C cannot be produced by a decrease in NADW production. Nor is it possible, from the perspective of $\delta^{13}C$, to regard Pacific deep water as a "downstream" alteration product of Antarctic deep water, as it is today. The occurrence of Antarctic water that is low in ^{13}C relative to the Pacific requires a major source of ^{13}C-enriched deep water — either in the North Pacific (as has often been suggested) or the Atlantic (a possibility we suggest below).

From the perspective of benthic $\delta^{13}C$ data, Southern Ocean chemistry, rather than simply being a slave to North Atlantic circulation, is an active player in the complex of physical and biological processes that redistribute carbon in the ocean-atmosphere system on ice age time scales. These processes would lead to changes in atmospheric CO_2 levels and therefore provide an early positive feedback in the climatic response to orbital forcing. However, one must bear in mind that our other nutrient tracer, benthic foraminiferal Cd/Ca, offers quite a different view. Glacial values of Cd/Ca in the deep Southern Ocean are not high compared to the deep eastern Pacific. Thus whatever mechanism creates unusually depleted ^{13}C values in benthic forams of the Southern Ocean does not affect the values of Cd/Ca [Boyle,

1992]. Furthermore, the Cd/Ca levels in the northwest Pacific are significantly lower than in the eastern equatorial Pacific, while the ^{13}C values are essentially the same in both areas [Keigwin, 1987; Boyle, 1992]. Thus the Cd/Ca evidence is supportive of a nutrient-depleted deep-water source in the northwest Pacific, while the ^{13}C evidence is not. Because these discrepancies are not understood, caution is necessary in evaluating the $\delta^{13}C$-based hypothesis presented below.

When considered at face value, the $\delta^{13}C$ data presented in this paper (variable 20) and the additional $\delta^{13}C$ data presented by Howard [1991] suggest that the preglacial and glacial Southern Ocean was a "carbon trap," with more ^{13}C-depleted CO_2 being sequestered in Antarctic deep water. This depletion might be explained by an increase in Antarctic biological production. But such an ecological explanation seems unlikely for two reasons. First, biogenic Si fluxes actually appear to have been lower in the glacial Antarctic than they are today, at least south of the present polar front [Mortlock et al., 1991; Bareille et al., 1991]. Second, the magnitude of any biological effect has to be evaluated in light of the vigorous overturn of modern Antarctic waters. Polar-nutrient box models indicate that only one phosphate molecule is removed from the polar surface box for every nine or so that pass through via the circulation [Toggweiler and Sarmiento, 1985]. Thus, even a doubling of the biological production is not going to have much of an impact unless the local overturning is also reduced.

In order to rationalize the Antarctic $\delta^{13}C$ data, we offer a carbon-trapping hypothesis for the deep Antarctic that depends on a diminished exchange with deep waters of the other oceans while biological production remains at more or less "normal" levels. Our carbon-trapping mechanism is driven by a northward shift in the latitude of the maximum southern hemisphere westerlies. A shift in the winds is assumed to be the cause of the preglacial shift of Antarctic fronts and water masses described above. Our mechanism involves a simple change in circulation and is independent of other changes associated with the shift in frontal position (e.g., changes in sea ice, biological production, or modewater formation).

The physical basis of this trapping mechanism is a unique dynamic constraint that operates in the latitude band of Drake Passage [Gill and Bryan, 1971]. Over most of the ocean, poleward flows in the ocean interior are maintained by east-west pressure gradients that build up against north-south continental barriers. Within the latitude band of Drake Passage, a net east-west pressure gradient cannot exist, except below the tops of deep topographic barriers. Thus a simple thermohaline circulation is prohibited, i.e., warm water in the upper ocean cannot simply flow poleward across the latitude band of Drake Passage in order to form new bottom water [Cox, 1989; Warren, 1990]. Meanwhile, the winds in the circumpolar belt push the surface waters in this latitude band northward. (The northward flow of surface water is not affected by the existence of Drake Passage because it is directly forced by the wind and is not geostrophically balanced.) The northward wind drift and the Drake Passage constraint combine to drive a deep poleward flow which enters the latitude band of Drake Passage below the deep topography. The winds, in effect, "pull" deep water poleward across the latitude band of Drake Passage. When this deep water is upwelled to the surface, it creates the weakly stratified and chemically homogeneous water column we see around Antarctica.

The pulling effect of the circumpolar westerlies may have an especially important impact on the Atlantic's overturning. Experiments with a global ocean circulation model suggest that the magnitude of the deep outflow from the Atlantic is proportional to the westerly wind stress at the latitude of the tip of South America [Toggweiler and Samuels, 1992]. The formation of dense water in the isolated basins of the North Atlantic may be a necessary precondition for an Atlantic overturning to exist, but wind stress in the southern hemisphere appears to determine the magnitude of the overturning and the volume of Atlantic water which actually flows into the Southern Ocean. The latitude of the tip of South America is a critical geographic position in these model results. The circumpolar westerlies induce upwelling and a northward surface drift over a wide latitude band. However, it is only the upwelling and northward drift initiated south of the tip of South America which must be balanced by a southward flow of deep water.

The fact that the axis of the maximum westerlies is now only a few degrees north of Drake Passage [Trenberth et al., 1990] is an important consideration in deducing how the exchange of deep water between the Antarctic and other oceans would vary over an ice age cycle. Geological data from the southern Indian Ocean (e.g., variable 7) indicate that this wind axis moves away from Drake Passage to its maximum northward position during a preglacial state [Howard and Prell, 1992]. A northward movement of the maximum westerlies would tend to reduce the critical wind stress at the tip of South America. According to the model results of Toggweiler and Samuels [1992], this would weaken the "pulling" effect that now draws deep water into the Antarctic region. Under these conditions, the relatively stagnant and isolated waters of the deep Antarctic could become a carbon trap as they accumulate respired CO_2 from the biological production in the overlying waters. Thus a northward shift in the preglacial position of the Antarctic fronts may be mechanistically consistent with a reduced flow of Atlantic deep water into the Antarctic Ocean and low $\delta^{13}C$ levels in Antarctic Bottom Water.

We speculate that a reduced wind-pulling effect might have another significant consequence. The

depth at which modern North Atlantic deepwater flows poleward (between 2000 and 4000 m) may be related to the fact that deep water is preferentially pulled poleward into the circumpolar belt; i.e., the weaker pulling effect of the circumpolar westerlies during the preglacial and glacial states could reduce the southward flow of the deepest North Atlantic deep water and may help explain the generally shallower position of high-^{13}C Atlantic deep water during these times (Figure 1). In any event, a shallower variety of North Atlantic deep water will have a more difficult time reaching the high latitudes of the Southern Ocean where it can be recycled into bottom water [Warren, 1990]. Instead, any high-^{13}C water emerging beyond the tip of Africa might simply flow eastward into the Indian and Pacific basins, bypassing the Antarctic entirely. Thus the same mechanism that traps low-^{13}C water in the Antarctic during the preglacial and glacial states might also provide a source of relatively high-^{13}C water to the Pacific. This would be sufficient to reverse the Antarctic-Pacific ^{13}C gradient (variable 20) without the necessity of forming a high-^{13}C deep water within the Pacific itself.

In our model of the major glaciation cycles, initial forcing toward this carbon-trapping response is provided by a reduction of heat transport that accompanies the reduced volume transport in the lower NADW. The geostrophic response to this thermal forcing is determined by westerly winds at the Drake Passage. We suggest that it is this local, geostrophic response, rather than the direct volumetric contribution by NADW, that dominates the carbon balance and traps carbon in the Southern Ocean. One argument for this point of view is provided by the phase measurements presented earlier (Figure 10). Our long record of deep Antarctic $\delta^{13}C$ depletion (variable 20) falls among the early responses, while our record of deep North Atlantic $\delta^{13}C$ depletion (variable 14) falls among the late responses, reaching its maximum depletion just after the ice maximum when the deep mixing front is at its northern extreme (Figure 6). Although the site of variable 14 may be too far north to sense an initial change in the $\delta^{13}C$ plume, the carbon isotopic evidence from this site seems to indicate that the main North Atlantic contribution to the Southern Ocean carbon balance does not come at the right time to explain much of the carbon trapping seen in the deep Antarctic.

6.5.3. *Glacial state.* As the northern ice sheets continue to grow [Denton and Hughes, 1981], they exert an ever stronger control on the position, speed, temperature, and water content of northern hemisphere winds. In turn, these atmospheric changes have a strong and immediate downwind effect both on the ocean and the continents [Manabe and Broccoli, 1985; Broccoli and Manabe, 1987]. As the ice sheets attain their maximum size in each cycle, the area that is influenced by cold, dry winds reaches its maximum for that cycle. In the boreal Atlantic, the ocean's response is to expand the area where wintertime convection occurs, and to intensify the ventilation of intermediate waters by processes analogous to those occurring today in the wintertime Labrador Sea. In reconstructions of the Atlantic at the LGM extreme of the 100-kyr ice volume cycle, we therefore see an expansion of $\delta^{13}C$-enriched intermediate waters (Figure 1).

In one geochemical model [Boyle, 1988], this redistribution of nutrients between intermediate and deep reservoirs will, on a time scale of many thousands of years, make a small contribution toward lowering the atmospheric CO_2. The time constant of alkalinity change that drives this response is therefore much longer than the century-scale time constant that controls the response to the Southern Ocean carbon-trapping mechanism discussed above. We conclude that one mechanism acts as an early and strong positive feedback, and that the other acts as a later and weaker positive feedback.

At the cyclic extreme represented by the ice maximum, and in portions of the northeast Atlantic where surface salinities are favorable, ventilation in the boreal ocean can apparently extend below intermediate depths [Duplessy et al., 1991b]. We suggest that these extreme conditions will produce a modest increase in heat export by the deeper layers of NADW compared to the heat export characteristic of a preglacial state. Eventually, this increase will lead to a warming of Antarctic waters, a reduction of Antarctic sea ice and a reduction in carbon trapping. However, the immediate effect of the ice volume maximum that defines a glacial state within each cycle is the eustatic lowering of sea level to its extreme position. At these extremes of the 100-kyr ice volume cycle, ice sheets become grounded on large areas of the continental shelf around the world [Solheim et al., 1990; Anderson and Thomas, 1991], thus setting the stage for a sudden, synchronous, and irreversible retreat that will affect ice sheets in both polar hemispheres [Hughes, 1987].

Although the evidence is only fragmentary, we think it worth considering the possibility that one of the processes that ventilate North Pacific intermediate waters might involve a mechanism broadly similar to the one we infer for the North Atlantic. At climatic extremes like the LGM, when the subpolar gyre expanded [Sancetta, 1979], glaciers grew on Kamchatka [Denton and Hughes, 1981], and polar air steered by ice sheets extended farther eastward, the production of intermediate water might have increased at sites along the Northwest Pacific rim [Reid, 1965; Talley, 1991]. Our $\Delta\delta^{13}C$ record (variable 10) offers some support for this idea by suggesting that the modest changes in the ventilation of intermediate water that occur in the eastern tropical Pacific are coherent with $\delta^{18}O$ in the 41- and 100-kyr cycles [Mix et al., 1991]. In the 41-kyr band, the in-

crease in ventilation is on phase with $\delta^{18}O$, but in the 100-kyr band, the phase increase is intermediate between the early and late response groups (Table 2).

6.5.4. *Deglacial state.* In response to a continuous increase in summer radiation in the Arctic, the atmosphere and surface ocean warm, evaporation increases, and snow fields shrink. In the Nordic Sea, the extent of sea ice is reduced. In boreal latitudes, the mass budgets of the ice sheets become negative, causing the Laurentide ice margin to retreat (Figure 13). Although initially the effect of this retreat on sea level is small, its effect on the wind field is significant because it drives warm, saline Atlantic water northward, thus increasing the exchange of waters with the Nordic Sea [Lehman et al., 1991; Rhines and Schopp, 1991]. This exchange provides heat that helps melt the ice sheets and supplies salt that increases convection. Because the longest time constants in this cluster of positive feedbacks are those involving the ice sheet margin, this initial part of the deglaciation process advances rather quickly. When a threshold is reached in the 100-kyr ice volume cycle, the Barents Sea and perhaps other marine-based ice sheets around the Arctic become unstable, triggering a significant deglaciation in and around the Nordic Sea [Jones and Keigwin, 1988; Vorren et al., 1988; Lehman et al., 1991]. As noted above, the sea level effects of this change would have an immediate impact on all ice sheets that are grounded below sea level [Weertman, 1974; Hughes, 1987].

With the invasion of salty Atlantic water into the Nordic Sea, the Nordic pump is turned on and the system returns to a two-pump mode. Because this mode shift occurs before the ice sheets have had a chance to retreat very far, a wind field that is still strongly influenced by the ice sheets would be expected to drive the boreal pump much faster than it does during an interglacial. Thus the total NADW export flux — and therefore the flux of heat to areas undergoing deglaciation in both hemispheres — would be at its cycle maximum early in the deglaciation [Shackleton et al., 1988; Duplessy et al., 1991b]. (This deduction can be tested against other observations when U/Th ages near 13 ka are available to compare with ^{14}C ages.) The warming of Antarctic subsurface waters would reduce the extent of sea ice, move the axis of maximum westerlies back toward the Drake Passage, reduce the production of Subantarctic mode waters, and lead quickly to a redistribution of nutrients among ocean reservoirs and an increase in atmospheric CO_2 [Labeyrie et al., 1986; Labracherie et al., 1989]. What had been a stately Milankovitch retreat now becomes a rout. The system returns rapidly to an interglacial state, and the cycle is complete.

6.6. *System Model*

We now attempt to explain the clustering of responses in the phase spectrum. Our modeling strategy is to postulate discrete sources of inertia that seem capable of pacing the responses along the causal pathways that are identified in our process model (Figure 3). We start by assuming that the 23- and 41-kyr cycles are the responses of a linear, single-exponential system with one input (radiation) and one output ($\delta^{18}O$). For these cycles, we have in fact good evidence from the coherency spectrum that the $\delta^{18}O$ ice-volume proxy is linear in the radiative forcing. If such a system is forced at frequency f, the phase lag (ϕ) depends on the nature of the system's response. We assume that this response can be characterized by a delay (d) and a mean time constant (T). Then $\phi = 2\pi f d + \arctan 2\pi f T$ [Jenkins and Watts, 1968]. If we also assume that $d = 0$, the observed phases at 23- and 41-kyr yield independent estimates of T (70 and 37 kyr for the two bands, respectively) which are not only much larger than values estimated by ice sheet models [Weertman, 1964], but which are inconsistent between the two cycles. However, if we solve simultaneously for d and T at both frequencies, the solution (d = 1 kyr and T = 17 kyr) gives phase lags (93° and 78°) that match rather well the lags observed in both cycles (87° and 80°). This estimate of the time constant (17 kyr) lies well within the theoretical range and matches an empirical estimate made by a different method [Imbrie and Imbrie, 1980].

We interpret the delay of 1 kyr as due to the largest source of inertia in an interacting cluster of initial-response mechanisms that includes variations in northern hemisphere snow fields, sea ice, winds, and ice sheet margins (Figure 13). On the model phase wheel in Figure 14, we designate this set of mechanisms as subsystem S_1 and its delayed response as R_1. Expressed as a phase angle, the delay is 16° at 23 kyr and 9° at 41 kyr. These values are therefore the phases our model predicts for the initial response of the climate system to radiative forcing in the 23- and 41-kyr bands. Since these initial responses are not observed in our long time series, we note that the four-state model used in Figure 3 to describe the system's evolution does not permit the display of the differences which must exist between initial and preglacial states. To do this, we would have to expand the number of end-member states from four to six.

So far, our analysis of the phase spectrum has been limited to the response of one variable, $\delta^{18}O$. We now examine all measured phases simultaneously. Displayed as vectors in Figure 10, these fall into two clusters, an early response group and a late response group. In a later paper we will examine the statistics in Table 2 in more detail and show that these observations are consistent with the hypothesis that, within each cycle and within the range of uncertainty produced by observational error and climatic noise, the system responses we measure in Table 2 occur at three discrete phase intervals that lag the postulated initial responses, R_1. In Figure 14, we

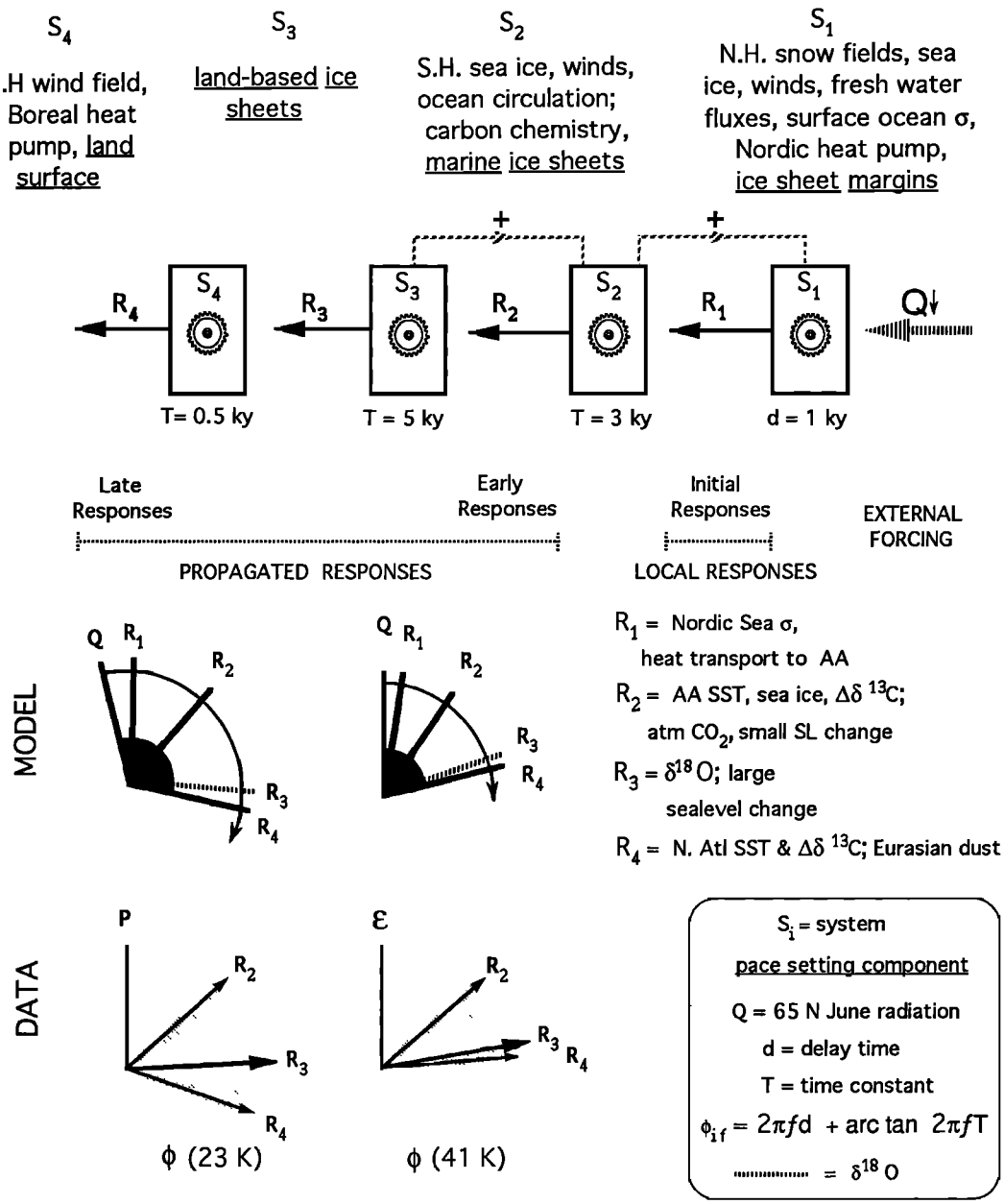

Fig. 14. Systems model of the 23-kyr and 41-kyr cycles. The model attempts to identify sources of inertia controlling the rate at which the local response to radiation is propagated through the system. Climate is modeled as a chain of subsystems S_i each having either a delay d or a time constant T. The initial response to radiation is propagated through the chain, the phase lag at each step i and frequency f being $2\pi fd$ or arc tan $2\pi fT$. These lags cumulate along the chain to yield the entire phase sequence. R_1 is identified as the set of initial responses; R_2 as the set of early responses; R_3 as ice volume ($\delta^{18}O$); and R_4 as the set of late responses. Feedback loops are shown by dashed lines. Within error bars, the model sequences match the observed responses R_2, R_3, and R_4 (Table 2).

designate as response group R_2 a set of early responses that includes southern hemisphere sea ice, SST, winds, ocean circulation and carbon chemistry; as R_3 the $\delta^{18}O$ (ice volume) response; and as R_4 the set of late responses that includes SST and ventilation in the boreal Atlantic as well as continental aridity. Shaded arcs represent confidence intervals with respect to R_3 ($\delta^{18}O$). The corresponding subsystems S_2, S_3, and S_4 are also defined in this figure.

The system as a whole can now be modeled as a chain of four subsystems S_i, each having a quantity of climatic inertia parameterized either as a delay d

or time constant T. We have already determined that the phase of the initial response to radiation, R_1, is controlled by a delay, d = 1 kyr. We now assume that the propagated responses are controlled at each step in the causal chain by a time constant. The numerical problem of accounting for the phase observations is thus reduced to finding three time constants which yield a cumulative pattern of responses that match the data. Because responses are calculated at two frequencies, the inverse problem is tightly constrained. For subsystems S_2, S_3, and S_4, our solution gives values of 3, 5, and 0.5 kyr, respectively. The predicted phase sequence just fits within the confidence intervals of the observations — provided we make a modest adjustment in the zero position of the forcing in the 23-kyr (precession) band.

Up to this point we have taken this to be the midmonth values for June 65°N [Berger, 1978a]. By shifting this arbitrary reference 15° (to June 1), the predicted values of the 23-kyr phase sequence fit the data. (The phase of the 41-kyr radiation cycle has a natural zero for all seasons and cannot be shifted.) In section 5.3 we noted that the phase of the SST response at 41°N in the precession band is essentially 180° out of phase with the June 1 radiation curve. This can be seen by comparing the phase of variable 6 (Figure 9a) with the phase of the radiative forcing in our model of the 23-kyr band (Figure 14).

In a later paper, we calculate values for the four inertial parameters in the 100-kyr cycle. These prove to be the same as values found here, except that the time constant for the ice sheets (S_3) is 15 kyr rather than 5 kyr. The implication here is that large ice sheets behave differently than smaller ones beyond some critical size.

Although the numerical problem of specifying a set of inertial parameters is easily solved for the linear case, the geophysical problem of identifying inertial sources in the real climate system presents a substantial challenge that is beyond the scope of this paper. The identifications made in Figure 14 should be considered speculations to guide future work.

One virtue of our system model is that it emphasizes two key roles that ice sheets play in the system's response over a glaciation cycle. The inertial role of the ice sheets in pacing the responses has long been understood. What has perhaps not been emphasized so clearly before is the active role that ice sheets play in driving responses farther down the causal chain (R_4) by steering and altering the properties of the winds.

7. CONCLUSIONS

1. Glaciation cycles with periods near 23,000 and 41,000 years have influenced virtually every part of the global climate system for well over 500,000 years. To first order, these cycles are continuous, linear responses to orbitally driven changes in the earth's radiation budget. This provides a rare opportunity to test models of the climate system's response to a known external forcing.

2. At least four end-member states are needed to describe the system's evolution: interglacial, preglacial, glacial, and deglacial. Displays using fewer end members give a distorted view of the glaciation process.

3. In both the 23- and 41-kyr cycles, the initial response to the forcing occurs in the Arctic, where changes in the fresh water budget modulate the production of the overflows from the Nordic Sea that entrain warm waters and export heat to the deep ocean. This initial response is propagated in an orderly progression of responses along causal pathways in the ocean and atmosphere. These responses arrive at different places at different times because sources of inertia that control the flow of climatic energy differ among the mechanisms that form these causal chains. The chain that begins with convection in the Nordic Sea quickly alters the extent of Antarctic sea ice. In turn, this forces a change in the patterns of atmospheric and oceanic flow and in the partitioning of carbon and nutrients among ocean reservoirs. These responses lead the ice sheets. On land and in the boreal ocean, another set of responses are on phase with or lag the ice sheets because they are driven by the ice sheets themselves through their influence on the wind field. These responses include the formation of upper NADW by convection in the open boreal Atlantic.

4. The $\delta^{13}C$ changes in the deep Antarctic reflect a redistribution of carbon and nutrients among ocean reservoirs that cannot be explained as the result of linear mixing between North Atlantic and Pacific sources. The Southern Ocean is apparently the site of an independent driving mechanism. Some combination of increased downward particle flux, and decreased mixing of deepwater masses with adjacent surface or deep waters must drive Southern Ocean carbon chemistry to the preglacial and glacial extremes suggested by ^{13}C data. We suggest a mechanism that emphasizes an exchange with adjacent oceans that is modulated by the geostrophic response to westerly winds at the Drake Passage. Whatever the mechanism, deep water of the Southern Ocean appears to act as a net dissolved carbon sink relative to the atmosphere and the rest of the ocean and does so early in the sequence of responses that leads the system toward a glacial state.

5. At least four different sources of climatic inertia with time constants ranging from 0.5 to 5 kyr are required to explain the clustering of responses in phase spectra of the 23- and 41-kyr cycles. Phases of responses in the 100-kyr cycle can be modeled by setting the 5-kyr parameter at 15 kyr.

6. As the system varies continuously but at different rates among the four extreme states, it exhibits shifts between two modes of ocean circulation. Each mode is identified with a particular combination of pathways in the Atlantic's warm-to-cold-water conversion process. Early in a deglaciation, the Nordic

and boreal mechanisms reinforce each other and drive the global overturning at its maximum rate for the cycle. Early in a preglaciation, the boreal mechanism operates alone at its minimum rate so that overturning is then at its minimum.

Acknowledgments. We are grateful to many people who have given us ideas and provided constructive criticism of earlier drafts of this paper. These include K. Aagaard, M. L. Bender, W. S. Broecker, K. Bryan, W. B. Curry, J.-C. Duplessy, R. G. Fairbanks, J. Farrell, A. L. Gordon, I. M. Held, T. Hughes, E. Jansen, L. D. Labeyrie, S. J. Lehman, S. Manabe, M. S. McCartney, D. W. Oppo, C. Sancetta, T. Sowers, and T. F. Stocker. We thank E. Bard, A. J. Broccoli, E. Jansen, N. K. Karpuz, and L. D. Keigwin for providing unpublished information. Much of the work reported here has been supported by a National Science Foundation grant to the multi-institutional SPECMAP project. This support includes SPECMAP grants ATM8812589 to Brown University (Imbrie and Prell); ATM8812640 to Oregon State University (Mix and Pisias); ATM8812637 to the Lamont-Doherty Geological Observatory, Columbia University (Kukla, Martinson, McIntyre); and ATM8812639 to the University of Wisconsin (Kutzbach). We also acknowledge NERC grant GR3/606 (Shackleton) and NSF support from the following grants: ATM8902849 and ATM8713227 to the University of Wisconsin (Kutzbach); OCE8810949 (Raymo) and ATM8703017 (Kukla) to LDGO; OCE8710168 to MIT (Boyle); ATM8706394 (Imbrie) and ATM8516140 (Imbrie and Shackleton, Dec. 1985 to Dec. 1990) to Brown University. A continuation of ATM8516140 (Jan. 1991 to) supported the senior author's work on this project. The quotation from Victor P. Starr is from Peixoto and Oort [1992].

REFERENCES

Aagaard, K., and E. C. Carmack, The role of sea ice and other fresh water in the Arctic circulation, *J. Geophys. Res., 94,* 14,485-14,498, 1989.

Aagaard, K., J. H. Swift, and E. C. Carmack, Thermohaline circulation in the Arctic Mediterranean seas, *J. Geophys. Res., 90,* 4833-4846, 1985.

Anderson, J. B., and M. A. Thomas, Marine ice-sheet decoupling as a mechanism for rapid, episodic sea-level change: The record of such events and their influence on sedimentation, in *The Record of Sea-Level Fluctuations,* edited by K. T. Biddle and W. Schlager, pp. 87-104, Elsevier Science, New York, 1991.

Bard, E., B. Hamelin, and R. G. Fairbanks, U-Th ages obtained by mass spectrometry in corals from Barbados: Sea level during the past 130,000 years, *Nature, 346,* 456-458, 1990a.

Bard, E., L. D. Labeyrie, J. J. Pichon, M. Labracherie, M. Arnold, J. Duprat, J. Moyes, and J.-C. Duplessy, The last deglaciation in the southern and northern hemispheres: A comparison based on oxygen isotopes, sea surface temperature estimates, and accelerator ^{14}C dating from deep-sea sediments, in *Geological History of the Polar Oceans: Arctic versus Antarctic,* edited by U. Bleil and J. Thiede, pp. 405-416, Kluwer Academic, Boston, Mass., 1990b.

Barnola, J. M., D. Raynaud, Y. S. Korotkevich, and C. Lorius, Vostok ice core provides 160,000-year record of atmospheric CO_2, *Nature, 329,* 408-414, 1987.

Bareille, G., M. Labracherie, L. D. Labeyrie, J. J. Pichon, and J.-L. Turon, Biogenic silica accumulation rate in the Holocene in the southeastern Indian Ocean, *Mar. Chem., 35,* 537-551, 1991.

Belanger, P. E., Paleo-oceanography of the Norwegian Sea during the past 130,000 years: coccolithophorid and foraminiferal data, *Boreas, 11,* 29-36, 1982.

Berger, A., Long-term variations of caloric insolation resulting from the Earth's orbital elements, *Quat. Res., 9,* 139-167, 1978a.

Berger, A., *A Simple Algorithm to Compute Long Term Variations of Daily or Monthly Insolation,* 39 pp., University Catholique de Louvain, Louvain, Belgium, 1978b.

Birchfield, G. E., and J. Weertman, Topography, albedo-temperature feedback, and climate sensitivity, *Science, 219,* 284-285, 1983.

Bleil, U., and G. Gard, Chronology and correlation of Quaternary magnetostratigraphy and nannofossil biostratigraphy in Norwegian-Greenland Sea sediments, *Geol. Rundsch, 78,* 1173-1187, 1989.

Boyle, E. A., Cadmium in benthic foraminifera and abyssal hydrography: Evidence for a 41 kyr obliquity cycle, in *Climate Processes and Climate Sensitivity,* edited by J. E. Hansen and T. Takahashi, pp. 360-368, AGU, Washington, D. C., 1984a.

Boyle, E. A., Sampling statistic limitations on benthic foraminifera chemical and isotopic data, *Mar. Geol., 58,* 213-224, 1984b.

Boyle, E. A., The role of vertical chemical fractionation in controlling late Quaternary atmospheric carbon dioxide, *J. Geophys. Res., 93,* 15,701-15,714, 1988.

Boyle, E. A., Quaternary deepwater paleoceanography, *Science, 249,* 863-870, 1990.

Boyle, E. A., Cadmium and $\delta^{13}C$ paleochemical ocean distributions during the Stage 2 glacial maximum, *Annu. Rev. Earth Planet. Sci., 20,* 245-287, 1992.

Boyle, E. A., and L. D. Keigwin, Deep circulation of the North Atlantic over the last 200,000 years: Geochemical evidence, *Science, 218,* 784-787, 1982.

Boyle, E. A., and L. D. Keigwin, Comparison of Atlantic and Pacific paleochemical records for the last 215,000 years: Changes in deep ocean circulation and chemical inventories, *Earth Planet. Sci. Lett., 76,* 135-150, 1985.

Boyle, E. A., and L. D. Keigwin, North Atlantic thermohaline circulation during the past 20,000 years linked to high-latitude surface temperature, *Nature, 330,* 35-40, 1987.

Broccoli, A. J., and S. Manabe, The influence of continental ice, atmospheric CO_2, and land albedo on the climate of the last glacial maximum, *Clim. Dyn., 1,* 87-99, 1987.

Broecker, W. S., Glacial to interglacial changes in ocean chemistry, *Prog. Oceanogr., 11,* 151-197, 1982.

Broecker, W. S., Some thoughts about the radiocarbon budget for the glacial Atlantic, *Paleoceanography, 4,* 213-220, 1989.

Broecker, W. S., Salinity history of the northern Atlantic during the last deglaciation, *Paleoceanography, 5,* 459-467, 1990.

Broecker, W. S., and G. H. Denton, The role of ocean-atmosphere reorganizations in glacial cycles, *Geochim. Cosmochim. Acta, 53,* 2465-2501, 1989.

Broecker, W. S., and T.-H. Peng, The cause of the glacial to interglacial atmospheric CO_2 change: A polar alkalinity hypothesis, *Global Biogeochem. Cycles, 3,* 215-239, 1989.

Broecker, W. S., and J. van Donk, Insolation changes, ice volumes, and the ^{18}O record in deep-sea cores, *Rev. Geophys., 8,* 169-197, 1970.

Broecker, W. S., D. M. Peteet, and D. Rind, Does the ocean-atmosphere system have more than one stable mode of operation?, *Nature, 315,* 21-26, 1985.

Budd, W. F., and P. Rayner, Modelling global ice and climate changes through the ice ages, *Ann. Glaciol., 14,* 23-27, 1990.

Budd, W. F., and I. N. Smith, Conditions for growth and retreat of the Laurentide Ice Sheet, *Geogr. Phys. Quat., 41,* 279-290, 1987.

Charles, C. D., and R. G. Fairbanks, Evidence from Southern Ocean sediments for the effect of North Atlantic deep-water flux on climate, *Nature, 355,* 416-419, 1992.

Clemens, S. C., and W. L. Prell, Late Pleistocene variability of Arabian Sea summer monsoon winds and continental aridity: Eolian records from the lithogenic component of deep-sea sediments, *Paleoceanography, 5,* 109-145, 1990.

Clemens, S. C, W. L. Prell, D. Murray, G. Shimmield, and G. Weedon, Forcing mechanisms of the Indian Ocean monsoon, *Nature, 353,* 720-725, 1991.

CLIMAP Project Members, Seasonal reconstructions of the Earth's surface at the last glacial maximum, *Geol. Soc. Am. Map and Chart Ser., 36,* 1981.

COHMAP Members, Climatic changes of the last 18,000 years: Observations and model simulations, *Science, 241,* 1043-1052, 1988.

Cox, M. D., An idealized model of the world ocean, Part I, The global-scale water masses, *J. Phys. Oceanogr., 19,* 1730-1752, 1989.

Crowley, T. J., Late Quaternary carbonate changes in the North Atlantic and Atlantic/Pacific comparisons, in *The Carbon Cycle and Atmospheric CO_2: Natural Variations Archean to Present, Geophys. Monogr. Ser.,* vol. 32, edited by E. Sundquist and W. S. Broecker, pp. 271-284, American Geophysical Union, Washington, D. C., 1985.

Curry, W. B., and T. J. Crowley, The $\delta^{13}C$ of equatorial Atlantic surface waters: Implications for ice age pCO_2 levels, *Paleoceanography, 2,* 489-517, 1987.

Curry, W. B., and G. P. Lohmann, Carbon isotopic changes in benthic foraminifera from the western South Atlantic: Reconstruction of glacial abyssal circulation patterns, *Quat. Res., 18,* 218-235, 1982.

Curry, W. B., J.-C. Duplessy, L. D. Labeyrie, and N. J. Shackleton, Changes in the distribution of $\delta^{13}C$ of deep water ΣCO_2 between the last glaciation and the Holocene, *Paleoceanography, 3,* 317-341, 1988.

DeBlonde, G., and W. R. Peltier, A one-dimensional model of continental ice volume fluctuations through the Pleistocene: Implications for the origin of the Mid-Pleistocene climate transition, *J. Clim., 4,* 318-344, 1991.

deMenocal, P. B., D. W. Oppo, R. G. Fairbanks, and W. L. Prell, Pleistocene $\delta^{13}C$ variability of North Atlantic intermediate water, *Paleoceanography, 7,* 229-250, 1992.

Denton, G. H., and T. J. Hughes, *The Last Great Ice Sheets,* 484 pp., Wiley-Interscience, New York, 1981.

Duplessy, J.-C., N. J. Shackleton, R. G. Fairbanks, L. D. Labeyrie, D. Oppo, and N. Kallel, Deepwater source variations during the last climatic cycle and their impact on the global deepwater circulation, *Paleoceanography, 3,* 343-360, 1988.

Duplessy, J. -C., E. Bard, M. Arnold, N. J. Shackleton, J. Duprat, and L. Labeyrie, How fast did the ocean-atmosphere system run during the last deglaciation?, *Earth Planet. Sci. Lett., 103,* 27-40, 1991a.

Duplessy, J.-C., L. Labeyrie, A. Juillet-Leclerc, F. Maitre, J. Duprat, and M. Sarnthein, Surface salinity reconstruction of the North Atlantic Ocean during the last glacial maximum, *Oceanol. Acta, 14,* 311-324, 1991b.

Emiliani, C., The cause of the ice ages, *Earth Planet. Sci. Lett., 37,* 349-354, 1978.

Fairbanks, R. G., A 17,000-year glacio-eustatic sea level record: Influence of glacial melting rates on the Younger Dryas event and deep-ocean circulation, *Nature, 342,* 637-642, 1989.

Gallée, H., J. P. van Ypersele, T. Fichefet, I. Marsi-

at, C. Tricot, and A. Berger, Simulation of the last glacial cycle by a coupled, sectorially averaged climate-ice sheet model, 2, Response to insolation and CO_2 variation, *J. Geophys. Res., 97,* 15,713-15,740, 1992.

Gill, A. E., and K. Bryan, Effects of geometry on the circulation of a three-dimensional southern-hemisphere ocean model, *Deep Sea Res., 18,* 685-721, 1971.

Gordon, A. L., and B. A. Huber, Southern Ocean winter mixed layer, *J. Geophys. Res., 95,* 11,655-11,672, 1990.

Grosswald, M. G., Late Weichselian ice sheet of northern Eurasia, *Quat. Res., 13,* 1-32, 1980.

Hays, J. D., J. Imbrie, and N. J. Shackleton, Variations in the Earth's orbit: Pacemaker of the ice ages, *Science, 194,* 1121-1132, 1976.

Howard, W. R., Oceanography of the Southern Ocean during the past 500,000 years, Ph.D. thesis, 345 pp., Brown Univ., Providence, R. I., Dec. 1991.

Howard, W. R., and W. L. Prell, Late Quaternary $CaCO_3$ preservation in the Southern Ocean (abstract), *Eos Trans. AGU, 71,* 1382, 1990.

Howard, W. R., and W. L. Prell, Late Quaternary surface circulation of the southern Indian Ocean and its relationship to orbital variations, *Paleoceanography, 7,* 79-117, 1992.

Hughes, T., Ice dynamics and deglaciation models when ice sheets collapsed, in *North America and Adjacent Oceans During the Last Deglaciation,* edited by W. F. Ruddiman and H. E. Wright Jr., pp. 183-220, Geological Society America, Boulder, Colo., 1987.

Hurdle, B. G., *The Nordic Seas,* 777 pp., Springer-Verlag, New York, 1986.

Imbrie, J., and J. Z. Imbrie, Modeling the climatic response to orbital variations, *Science, 207,* 943-953, 1980.

Imbrie, J., J. D. Hays, D. G. Martinson, A. McIntyre, A. C. Mix, J. J. Morley, N. G. Pisias, W. L. Prell, and N. J. Shackleton, The orbital theory of Pleistocene climate: Support from a revised chronology of the marine $\delta^{18}O$ record, in *Milankovitch and Climate, Part 1,* edited by A. L. Berger et al., pp. 269-305, D. Riedel, Hingham, Mass., 1984.

Imbrie, J., A. McIntyre, and A. Mix, Oceanic response to orbital forcing in the late Quaternary: Observational and experimental strategies, in *Climate and Geo-sciences,* edited by A. Berger et al., pp. 121-164, Kluwer Academic, Boston, Mass., 1989.

Jenkins, G. M., and D. G. Watts, *Spectral Analysis and Its Applications,* 525 pp., Holden-Day, San Francisco, Calif., 1968.

Jones, G. A., Spatial and temporal distribution of Laurentide and Fennoscandian meltwater during the last deglaciation, *Nor.Geol.Tidsskr., 71,* 145-148, 1991.

Jones, G. A., and L. D. Keigwin, Evidence from Fram Strait (78°N) for early deglaciation, *Nature, 336.* 56-59, 1988.

Jones, G. A., D. A. Johnson, and W. B. Curry, High-resolution stratigraphy in Late Pleistocene/Holocene sediments of the Vema Channel, *Mar. Geol., 58,* 59-87, 1984.

Karpuz, N. K., and E. Jansen, A high resolution diatom record of the last deglaciation from the SE Norwegian Sea: Documentation of rapid climatic changes, *Paleoceanography, 7,* 499-520, 1992.

Karpuz, N. K., and H. Schrader, Surface sediment diatom distribution and Holocene paleotemperature variations in the Greenland, Iceland and Norwegian Sea, *Paleoceanography, 5,* 557-580, 1990.

Keffer, T., D. G. Martinson, and B. H. Corliss, The position of the Gulf Stream during Quaternary glaciations, *Science, 241,* 440-442, 1988.

Keigwin, L. D., North Pacific deep water formation during the latest glaciation, *Nature, 330,* 362-364, 1987.

Keigwin, L. D., G. A. Jones, S. J. Lehman, and E. A. Boyle, Deglacial meltwater discharge, North Atlantic deep circulation, and abrupt climate change, *J. Geophys. Res., 96,* 16,811-16,828, 1991.

Kellogg, T. B., Late Quaternary climatic changes: Evidence from deep-sea cores of Norwegian and Greenland seas, in *Investigation of Late Quaternary Paleoceanography and Paleoclimatology,* edited by R. M. Cline and J. D. Hays, pp. 77-110, Geological Society of America, Boulder, Colo., 1976.

Kellogg, T. B., J. C. Duplessy, and N. J. Shackleton, Planktonic foraminiferal and oxygen isotopic stratigraphy and paleoclimatology of Norwegian deep-sea cores, *Boreas, 7,* 61-73, 1978.

Kipp, N. G., New transfer function for estimating past sea-surface conditions from sea-bed distribution of planktonic foraminiferal assemblages in the North Atlantic, in *Investigation of Late Quaternary Paleoceanography and Paleoclimatology,* edited by R. M. Cline and J. D. Hays, pp. 3-42, Geological Society of America, Boulder, Colo., 1976.

Kroopnick, P., The distribution of ^{13}C and ΣCO_2 in the world oceans, *Deep Sea Res., 32,* 57-84, 1985.

Kukla, G., A. Berger, R. Lotti, and J. Brown, Orbital signature of interglacials, *Nature, 290,* 295-300, 1981.

Kukla, G., Z. S. An, J. L. Melice, J. Gavin, and J. L. Xiao, Magnetic susceptibility record of Chinese loess, *Trans. R. Soc. Edinburgh Earth Sci., 81,* 263-288, 1990.

Kutzbach, J. E., and R. G. Gallimore, Sensitivity of a coupled atmosphere/mixed-layer ocean model to changes in orbital forcing at 9000 years B.P., *J. Geophys. Res., 93,* 803-821, 1988.

Kutzbach, J. E., and P. J. Guetter, The influence of

changing orbital parameters and surface boundary conditions on climate simulations for the past 18,000 years, *J. Atmos. Sci., 43,* 1726-1759, 1986.

Labeyrie, L. D., J. J. Pichon, M. Labracherie, P. Ippolito, J. Duprat, and J.-C. Duplessy, Melting history of Antarctica during the past 60,000 years, *Nature, 322,* 701-706, 1986.

Labeyrie, L. D., J.-C. Duplessy, and P. L. Blanc, Variations in mode of formation and temperature of oceanic deep waters over the past 125,000 years, *Nature, 327,* 477-482, 1987.

Labracherie, M., L. D. Labeyrie, J. Duprat, E. Bard, M. Arnold, J. J. Pichon, and J.-C. Duplessy, The last deglaciation in the Southern Ocean, *Paleoceanography, 4,* 629-638, 1989.

Lehman, S. J., and L. D. Keigwin, Sudden changes in North Atlantic circulation during the last deglaciation, *Nature, 356,* 757-762, 1992a.

Lehman, S. J., and L. D. Keigwin, Deep circulation revisited, *Nature, 358,* 197-198, 1992b.

Lehman, S. J., G. A. Jones, L. D. Keigwin, E. S. Andersen, G. Butenko, and S.-R. Østmo, Initiation of Fennoscandian ice-sheet retreat during the last deglaciation, *Nature, 349,* 513-516, 1991.

Le Treut, H., and M. Ghil, Orbital forcing, climatic interactions, and glaciation cycles, *J. Geophys. Res., 88,* 5167-5190, 1983.

Maasch, K. A., and B. Saltzman, A low-order dynamical model of global climatic variability over the full Pleistocene, *J. Geophys. Res., 95,* 1955-1963, 1990.

Manabe, S., and A. J. Broccoli, The influence of continental ice sheets on the climate of an ice age, *J. Geophys. Res., 90,* 2167-2190, 1985.

Martinson, D. G., Evolution of the Southern Ocean winter mixed layer and sea ice: Open ocean deepwater formation and ventilation, *J. Geophys. Res., 95,* 11,641-11,654, 1990.

Martinson, D. G., N. G. Pisias, J. D. Hays, J. Imbrie, T. C. Moore, and N. J. Shackleton, Age dating and the orbital theory of the ice ages: Development of a high-resolution 0 to 300,000-year chronostratigraphy, *Quat. Res., 27,* 1-30, 1987.

McCartney, M. S., The subtropical recirculation of Mode Waters, *J. Mar. Res., 40, suppl.,* 427-464, 1982.

McCartney, M. S., Recirculating components to the deep boundary current of the northern North Atlantic, *Prog. Oceanog., 29,* 283-383, 1992.

McCartney, M. S., and L. D. Talley, The subpolar Mode Water of the North Atlantic Ocean, *J. Phys. Oceanogr., 12,* 1169-1188, 1982.

McCartney, M. S., and L. D. Talley, Warm-to-cold water conversion in the northern North Atlantic Ocean, *J. Phys. Oceanogr., 14,* 922-935, 1984.

McIntyre, A., N. G. Kipp, A. W. H. Be, T. Crowley, T. Kellogg, J. V. Gardner, W. Prell, and W. F. Ruddiman, Glacial North Atlantic 18,000 years ago: A CLIMAP reconstruction, in *Investigation of Late Quaternary Paleoceanography and Paleoclimatology*, edited by R. M. Cline and J. D. Hays, pp. 43-76, Geological Society of America, Boulder, Colo., 1976.

McIntyre, A., W. F. Ruddiman, K. Karlin, and A. C. Mix, Surface water response of the equatorial Atlantic Ocean to orbital forcing, *Paleoceanography, 4,* 19-55, 1989.

Meskó, A., *Digital Filtering Applications in Geophysical Exploration for Oil,* 636 pp., John Wiley, New York, 1984.

Mesolella, K. J., R. K. Matthews, W. S. Broecker, and D. L. Thurber, The astronomical theory of climatic change: Barbados data, *J. Geol., 77,* 250-274, 1969.

Milankovitch, M., *Mathematische Klimalehre und Astronomische Theorie der Klimaschwankungen,* 176 pp., Gebruder Borntraeger, Berlin, 1930.

Mitchell, J. F. B., N. S. Grahame, and K. J. Needham, Climate simulations for 9000 years before present: Seasonal variations and effect of the Laurentide ice sheet, *J. Geophys. Res., 93,* 8283-8303, 1988.

Mix, A. C., N. G. Pisias, R. Zahn, W. Rugh, C. Lopez, and K. Nelson, Carbon-13 in Pacific deep and intermediate waters, 0-370 ka: Implications for ocean circulation and Pleistocene CO_2, *Paleoceanography, 6,* 205-226, 1991.

Molfino, B., N. G. Kipp, and J. J. Morley, Comparison of foraminiferal, coccolithophorid, and radiolarian paleotemperature equations: Assemblage coherency and estimate concordancy, *Quat. Res., 17,* 279-313, 1982.

Morley, J. J., Variations in high-latitude oceanographic fronts in the southern Indian Ocean: An estimation based on faunal changes, *Paleoceanography, 4,* 547-554, 1989a.

Morley, J. J., Radiolarian-based transfer functions for estimating paleoceanographic conditions in the south Indian Ocean, *Mar. Micropaleontol., 13,* 293-307, 1989b.

Mortlock, R. A., C. D. Charles, P. N. Froelich, M. A. Zibello, J. Saltzman, J. D. Hays, and L. H. Burckle, Evidence for lower productivity in the Antarctic Ocean during the last glaciation, *Nature, 351,* 220-223, 1991.

Mysak, L. A., D. K. Manak, and R. F. Marsden, Sea-ice anomalies observed in the Greenland and Labrador seas during 1901-1984 and their relation to an interdecadal Arctic climate cycle, *Clim. Dyn., 5,* 111-133, 1990.

Neftel, A., H. Oeschger, J. Schwander, B. Stauffer, and R. Zumbrunn, Ice core sample measurements give atmospheric CO_2content during the past 40,000 yr, *Nature, 295,* 220-223, 1982.

Oglesby, R. J., Relationships between sea ice extent and oceanic and atmospheric circulations (abstract), *Eos Trans. AGU, 71,* 1368, 1990.

Oppo, D. W., R. G. Fairbanks, A. L. Gordon, and N. J. Shackleton, Late Pleistocene Southern Ocean

$\delta^{13}C$ variability, *Paleoceanography, 5,* 43-54, 1990.

Peixoto, J. P., and A. H. Oort, *Physics of Climate*, 520 pp., Am. Inst. of Physics, New York, 1992.

Peterson, L. C., and N. B. Cofer-Shabica, Brunhes Chron records of sedimentation and abyssal paleocirculation in the Venezuela Basin, eastern Caribbean Sea, *Geol. Soc. Am. Abstr. Programs, 19,* 804, 1987.

Petit, J. R., L. Mounier, J. Jouzel, Y. S. Korotkevich, V. I. Kotlyakov, and C. Lorius, Palaeoclimatological and chronological implications of the Vostok core dust record, *Nature, 343,* 56-58, 1990.

Pichon, J. J., M. Labracherie, L. D. Labeyrie, and J. Duprat, Transfer functions between diatom assemblages and surface hydrology in the Southern Ocean, *Paleogeogr. Paleoclimatol. Paleoecol., 61,* 79-95, 1987.

Pichon, J. J., L. D. Labeyrie, G. Bareille, M. Labracherie, J. Duprat, and J. Jouzel, Surface temperature changes in the high-latitudes of the southern hemisphere over the last glacial-interglacial cycle, *Paleoceanography, 7,* 289-318, 1992.

Prell, W. L., *The Stability of Low-Latitude Sea-Surface Temperatures: An Evaluation of the CLIMAP Reconstruction With Emphasis on the Positive SST Anomalies*, 60 pp., U.S. Department of Commerce, Washington, D. C., 1985.

Prell, W. L., and J. E. Kutzbach, Monsoon variability over the past 150,000 years, *J. Geophys. Res., 92,* 8411-8425, 1987.

Prell, W. L., W. H. Hutson, and D. F. Williams, The subtropical convergence and late Quaternary circulation in the southern Indian Ocean, *Mar. Micropaleontol., 4,* 225-234, 1979.

Prell, W. L., J. Imbrie, D. G. Martinson, J. J. Morley, N. G. Pisias, N. J. Shackleton, and H. F. Streeter, Graphic correlation of oxygen isotope stratigraphy: Application to the Late Quaternary, *Paleoceanography, 1,* 137-162, 1986.

Rasmusson, E. M., and T. H. Carpenter, Variations in tropical sea surface temperature and surface wind fields associated with the Southern Oscillation/El Niño, *Mon. Weather Rev., 110,* 354-384, 1982.

Raymo, M. E., W. F. Ruddiman, N. J. Shackleton, and D. W. Oppo, Evolution of Atlantic-Pacific $\delta^{13}C$ gradients over the last 2.5 m.y., *Earth Planet. Sci. Lett., 97,* 353-368, 1990.

Reid, J. L., *Intermediate Waters of the Pacific Ocean*, 85 pp., Johns Hopkins Press, Baltimore, Md., 1965.

Reid, J. L., and R. J. Lynn, On the influence of the Norwegian-Greenland and Weddell seas upon the bottom waters of the Indian and Pacific oceans, *Deep Sea Res., 18,* 1063-1088, 1971.

Rhines, P. B., and R. Schopp, The wind-driven circulation: Quasi-geostrophic simulations and theory for nonsymmetric winds, *J. Phys. Oceanogr., 21,* 1438-1469, 1991.

Rind, D., D. Peteet, and G. Kukla, Can Milankovitch orbital variations initiate the growth of ice sheets in a general circulation model?, *J. Geophys. Res., 94,* 12,851-12,871, 1989.

Rintoul, S. R., South Atlantic interbasin exchange, *J. Geophys. Res., 96,* 2675-2692, 1991.

Royer, J. F., M. Deque, and P. Pestiaux, A sensitivity experiment to astronomical forcing with a spectral GCM: Simulation of the annual cycle at 125,000 B.P. and 115,000 B.P., in *Milankovitch and Climate*, edited by A. L. Berger et al., pp. 733-763, D. Reidel, Hingham, Mass., 1984.

Ruddiman, W. F., and A. McIntyre, Oceanic mechanism for amplification of the 23,000-year ice-volume cycle, *Science, 212,* 617-627, 1981.

Ruddiman, W. F., and A. McIntyre, Ice-age thermal response and climatic role of the surface Atlantic Ocean, 40°N to 63°N, *Geol. Soc. Am. Bull., 95,* 381-396, 1984.

Ruddiman, W. F., M. E. Raymo, D. G. Martinson, B. M. Clement, and J. Backman, Pleistocene evolution: Northern hemisphere ice sheets and North Atlantic Ocean, *Paleoceanography, 4,* 353-412, 1989.

Sancetta, C., Oceanography of the North Pacific during the last 18,000 years: Evidence from fossil diatoms, *Mar. Micropaleontol., 4,* 103-123, 1979.

Shackleton, N. J., Carbon-13 in *Uvigerina*: Tropical rainforest history and the equatorial Pacific carbonate dissolution cycles, in *The Fate of Fossil Fuel CO_2 in the Oceans*, edited by N. R. Andersen and A. Malahoff, pp. 401-427, Plenum, New York, 1977.

Shackleton, N. J., Oxygen isotopes, ice volume and sea level, *Quat. Sci. Rev., 6,* 183-190, 1987.

Shackleton, N. J., and N. D. Opdyke, Oxygen isotope and paleomagnetic stratigraphy of equatorial Pacific core V28-238: Oxygen isotope temperatures and ice volumes on a 10^5 year and 10^6 year scale, *Quat. Res., 3,* 39-55, 1973.

Shackleton, N. J., and N. G. Pisias, Atmospheric carbon dioxide, orbital forcing, and climate, in *The Carbon Cycle and Atmospheric CO_2: Natural Variations Archean to Present, Geophys. Monogr. Ser.*, vol. 32, edited by E. Sundquist and W. S. Broecker, pp. 303-317, AGU, Washington, D. C., 1985.

Shackleton, N. J., J. Imbrie, and M. A. Hall, Oxygen and carbon isotope record of East Pacific core V19-30: Implications for the formation of deep water in the Late Pleistocene North Atlantic, *Earth Planet. Sci. Lett., 65,* 233-244, 1983.

Shackleton, N. J., J.-C. Duplessy, M. Arnold, P. Maurice, M. A. Hall, and J. Cartlidge, Radiocarbon age of last glacial Pacific deep water, *Nature, 335,* 708-711, 1988.

Short, D. A., J. G. Mengel, T. J. Crowley, W. T. Hyde, and G. R. North, Filtering of Milankovitch cycles by Earth's geography, *Quat. Res., 35,* 157-173, 1991.

Solheim, A., L. Russwurm, A. Elverhoi, and M. N.

Berg, Glacial geomorphic features in the northern Barents Sea: direct evidence for grounded ice and implications for the pattern of deglaciation and late glacial sedimentation, in *Glacimarine Environments: Processes and Sediments*, edited by J. A. Dowdeswell and J. D. Scourse, pp. 253-268, Geological Society, Spec. Pub. 53, London, 1990.

Sowers, T., M. Bender, D. Raynaud, Y. S. Korotkevich, and J. Orchardo, The $\delta^{18}O$ of atmospheric O_2 from air inclusions in the Vostok ice core: Timing of CO_2 and ice volume changes during the penultimate deglaciation, *Paleoceanography*, *6*, 679-696, 1991.

Stocker, T. F., D. G. Wright, and W. S. Broecker, The influence of high-latitude surface forcing on the global thermohaline circulation, *Paleoceanography*, in press, 1992.

Stuiver, M., T. F. Braziunas, B. Becker, and B. Kromer, Climatic, solar, oceanic, and geomagnetic influences on Late-Glacial and Holocene atmospheric $^{14}C/^{12}C$ change, *Quat. Res.*, *35*, 1-24, 1991.

Sundquist, E. T., and W. S. Broecker (Eds.), *The Carbon Cycle and Atmospheric CO_2: Natural Variations Archean to Present, Geophys. Monogr. Ser.*, vol. 32, 627 pp., AGU, Washington, D. C., 1985.

Swift, J. H., and K. Aagaard, Seasonal transitions and water mass formation in the Iceland and Greenland seas, *Deep Sea Res. Ser. A, 28*, 1107-1129, 1981.

Talley, L. D., An Okhotsk Sea water anomaly: Implications for ventilation in the North Pacific, *Deep Sea Res.*, *38*, 171-190, 1991.

Toggweiler, J. R., and B. Samuels, Is the magnitude of the deep outflow from the Atlantic Ocean actually governed by southern hemisphere winds?, in *The Global Carbon Cycle*, edited by M. Heimann, Springer-Verlag, New York, in press, 1992.

Toggweiler, J. R., and J. L. Sarmiento, Glacial to interglacial changes in atmospheric carbon dioxide: The critical role of ocean surface water in high latitudes, in *The Carbon Cycle and Atmospheric CO2: Natural Variations Archean to Present, Geophys. Monogr. Ser.*, vol. 32, edited by E. Sundquist and W. S. Broecker, pp. 163-184, AGU, Washington, D. C., 1985.

Toggweiler, J. R., K. Dixon, and K. Bryan, Simulations of radiocarbon in a coarse-resolution world ocean model, 1, Steady-state pre-bomb distributions, *J. Geophys. Res.*, *94*, 8217-8242, 1989.

Toggweiler, J. R., K. Dixon, and W. S. Broecker, The Peru upwelling and the ventilation of the South Pacific thermocline, *J. Geophys. Res*, *96*, 20,467-20,497, 1991.

Trenberth, K. E., W. G. Large, and J. G. Olson, The mean annual cycle in global ocean wind stress, *J. Phys. Oceanogr.*, *20*, 1742-1760, 1990.

Veum, T., E. Jansen, M. Arnold, I. Beyer, and J.-C. Duplessy, Water mass exchange between the North Atlantic and the Norwegian Sea during the past 28,000 years, *Nature*, *356*, 783-785, 1992.

Vorren, T. O., M. Hald, and E. Lebesbye, Late Cenozoic environments in the Barents Sea, *Paleoceanography*, *3*, 601-612, 1988.

Warren, B. A., Suppression of deep oxygen concentrations by Drake Passage, *Deep Sea Res.*, *37*, 1899-1907, 1990.

Weertman, J., Rate of growth or shrinkage of nonequilibrium ice sheets, *J. Glaciol.*, *5*, 145-158, 1964.

Weertman, J., Stability of the junction of an ice sheet and ice shelf, *J. Glaciol.*, *13*, 3-11, 1974.

Weyl, P. K., The role of the oceans in climatic change: A theory of the ice ages, *Meteorol. Monogr.*, *8*, 37-62, 1968.

Worthington, L. V., *On the North Atlantic Circulation*, 110 pp., Johns Hopkins University Press, Baltimore, Md., 1976.

Wunsch, C., An eclectic Atlantic Ocean circulation model, Part I, The meridional flux of heat, *J. Phys. Oceanogr.*, *14*, 1712-1733, 1984.

E. A. Boyle and M. E. Raymo, Department of Earth, Atmospheric, and Planetary Sciences, Massachusetts Institute of Technology, Cambridge, MA 02139.

S. C. Clemens, A. Duffy, J. Imbrie, and W. L. Prell, Department of Geological Sciences, Brown University, Providence, RI 02912.

W. R. Howard, G. Kukla, D. G. Martinson, A. McIntyre, B. Molfino, and J. Morley, Lamont-Doherty Geological Observatory of Columbia University, Palisades, NY 10964.

J. Kutzbach, Center for Climatic Research and Space Science, University of Wisconsin, Madison, WI 53706.

A. C. Mix and N. G. Pisias, College of Oceanography, Oregon State University, Corvallis, OR 97331.

L. C. Peterson, Rosenstiel School of Marine and Atmospheric Science, University of Miami, Miami, FL 33149.

N. J. Shackleton, Godwin Laboratory for Quaternary Research, Cambridge CB2 3RS, United Kingdom.

J. R. Toggweiler, Geophysical Fluid Dynamics Laboratory, NOAA, Princeton, NJ 08542.

(Received May 22, 1992;
revised September 17, 1992;
accepted September 17, 1992.)